iScience

CellPress
OPEN ACCESS

Article

The long non-coding RNA *CDK6-AS1* overexpression impacts on acute myeloid leukemia differentiation and mitochondrial dynamics

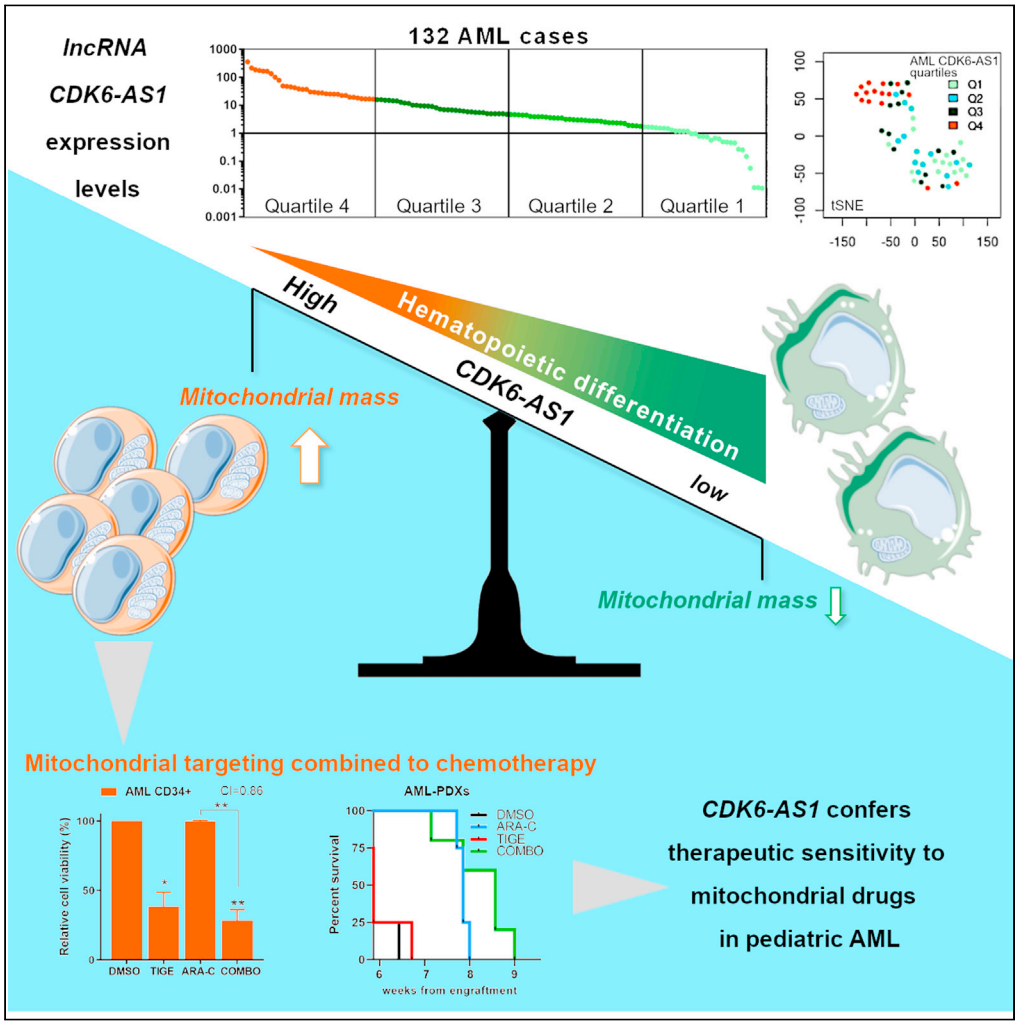

Elena Porcù, Maddalena Benetton, Valeria Bisio, ..., Dinesh S. Rao, Franco Locatelli, Martina Pigazzi

martina.pigazzi@unipd.it

Highlights

CDK6-AS1 acts in concert with *CDK6*

High *CDK6-AS1* levels trigger RUNX1 early differentiation arrest in myeloid cells

CDK6-AS1 controls mitochondrial mass of AML blasts

CDK6-AS1 levels impact on mitochondrial-targeted agents sensitivity

Porcù et al., iScience 24, 103350
November 19, 2021
https://doi.org/10.1016/j.isci.2021.103350

iScience

CellPress
OPEN ACCESS

Article

The long non-coding RNA *CDK6-AS1* overexpression impacts on acute myeloid leukemia differentiation and mitochondrial dynamics

Elena Porcù,[1,8] Maddalena Benetton,[1,8] Valeria Bisio,[1,8,9] Ambra Da Ros,[1] Claudia Tregnago,[1] Giulia Borella,[1] Carlo Zanon,[2] Matteo Bordi,[3,4] Giuseppe Germano,[2] Sabrina Manni,[5] Silvia Campello,[3] Dinesh S. Rao,[6] Franco Locatelli,[7] and Martina Pigazzi[1,2,10,*]

SUMMARY

Patients with acute myeloid leukemia (AML) carrying high-risk genetic lesions or high residual disease levels after therapy are particularly exposed to the risk of relapse. Here, we identified the long non-coding RNA *CDK6-AS1* able to cluster an AML subgroup with peculiar gene signatures linked to hematopoietic cell differentiation and mitochondrial dynamics. *CDK6-AS1* silencing triggered hematopoietic commitment in healthy CD34+ cells, whereas in AML cells the pathological undifferentiated state was rescued. This latter phenomenon derived from RUNX1 transcriptional control, responsible for the stemness of hematopoietic precursors and for the block of differentiation in AML. By *CDK6-AS1* silencing *in vitro*, AML mitochondrial mass decreased with augmented pharmacological sensitivity to mitochondria-targeting drugs. *In vivo*, the combination of tigecycline and cytarabine reduced leukemia progression in the AML-PDX model with high *CDK6-AS1* levels, supporting the concept of a mitochondrial vulnerability. Together, these findings uncover *CDK6-AS1* as crucial in myeloid differentiation and mitochondrial mass regulation.

INTRODUCTION

Pediatric acute myeloid leukemia (AML) is a molecularly heterogeneous disorder characterized by a large number of chromosomal translocations, resulting in the production of chimeric proteins, which confer a block of differentiation and an abnormal proliferation potential to hematopoietic stem cells. In the last decade, pediatric trials have incorporated numerous markers useful for stratification of patients in different risk groups (Bacher et al., 2014; Buldini et al., 2017; Inaba et al., 2012; Jongen-Lavrencic et al., 2018; Pession et al., 2013; Pigazzi et al., 2015; Rubnitz et al., 2010; Zwaan et al., 2015). Nevertheless, current diagnostic protocols partially fail to detect poor-risk patients (McNeer et al., 2019), suggesting the need to implement functional markers and treatments to more efficiently eradicate leukemia stem cells, whose survival and escape from the lytic action of cytotoxic agents are thought to be a major cause of treatment failure (Ng et al., 2016). Genome-scale studies have identified potentially targetable mutations in adult *de novo* AML (Papaemmanuil et al., 2016), whereas no remarkable driver mutations have been found in pediatric AML (Bolouri et al., 2018). Indeed, much AML research has focused on somatic mutations in protein coding genes, with few efforts in understanding the role played by long non-coding RNAs (lncRNAs). Recently, lncRNAs have been linked to several pathways in physiological cell biology and cancer, with recent findings demonstrating their aberrant hyper-activation (Quinn et al., 2016) leading to resistance mechanisms in different neoplasia, including acute leukemia (Bester et al., 2018; Salmena et al., 2011; Schmitt and Chang, 2016). LncRNAs are transcripts of more than 200 nucleotides, which can be localized into the nucleus or cytoplasm, playing diverse roles, acting as intergenic transcripts, enhancers, sense/antisense transcripts, regulators of nuclear domains (Deveson et al., 2017; Dykes and Emanueli, 2017), and transcriptional regulators both *in cis* or *trans* (Quinn et al., 2016). In this study, we focused on a lncRNA, known as *CDK6-AS1* (LOC101927497), to define its contribution to AML pathogenesis, since it was previously prioritized from differentially expressed lncRNAs and mRNAs in acute lymphoblastic leukemia (Fernando et al., 2015), as well as in human gastric epithelial tumorigenesis (Luo et al., 2018).

We dissected the role of *CDK6-AS1* in AML samples and in healthy CD34+ hematopoietic cells discovering its transcriptional activation and regulatory action over the chromosomally adjacent gene *CDK6*. This

[1]Pediatric Hematology, Oncology and Hematopoietic Cell&Gene Therapy Division of Women's and Children's Health Department, University-Hospital of Padova, Via N. Giustiniani, 3, 35128 Padova, Italy

[2]Pediatric Onco-Hematology, Stem Cell Transplant and Gene Therapy Laboratory, Istituto di Ricerca Pediatrica - Città della Speranza, 35127 Padova, Italy

[3]Department of Biology, University of Rome Tor Vergata, 00133 Rome, Italy

[4]Department of Pediatric Hemato-Oncology and Cell and Gene Therapy, IRCCS Bambino Gesù Children's Hospital, 00143 Rome, Italy

[5]Department of Medicine, Hematology and Clinical Immunology Branch, University of Padova, Padova, and Veneto Institute of Molecular Medicine (VIMM), 35129 Padova, Italy

[6]Department of Pathology and Laboratory Medicine, UCLA, Los Angeles, CA 90095, USA

[7]Department of Pediatric Hematology and Oncology, IRCCS Bambino Gesù Children's Hospital, Sapienza University of Rome, 00165 Roma, Italy

[8]These authors contributed equally

[9]Present address: Université de Paris, Institut de Recherche Saint Louis, EMiLy, Inserm U1160, 75010 Paris, France

[10]Lead contact

*Correspondence: martina.pigazzi@unipd.it

https://doi.org/10.1016/j.isci.2021.103350

network is able to impair the hematopoietic differentiation process through RUNX1 signaling and maintain an aberrant mitochondrial status. These latter findings were recognized in patients with AML with the highest *CDK6-AS1* expression, who might be included in a subgroup of cases with mitochondrial vulnerabilities to be exploited. Hence, *CDK6-AS1* levels arise as unique molecular determinant, which characterize those cases that, both in *in vitro* and *in vivo* experiments, proved to benefit from a mitochondrial-oriented therapeutic strategy.

RESULTS

CDK6-AS1 expression distinguishes a subgroup of patients with AML

We retrospectively analyzed the expression of the lncRNA *CDK6-AS1* in leukemia blasts of 132 pediatric patients with *de novo* AML enrolled in the AIEOP AML 2002/01 trial (Pession et al., 2013) harboring different genetic abnormalities including *CBF* rearrangements, i.e., t(8;21)*RUNX1-RUNX1T1* and inv(16) *CBFB-MYH11* (n = 20), *MLL*-translocations (n = 37), *NUP98*-translocations (n = 15), *FLT3*-ITD (n = 15), rare translocations (n = 9), and 36 patients without any recurrent molecular lesion (see Table S1A). Overall, *CDK6-AS1* expression was heterogeneous but significantly higher (*p value<0.05) in all AML samples when compared with healthy mononuclear cells from cord blood (used as calibrator, RQ = 1, see Figure S1A) and with healthy bone marrow (HBM, see Figure S1B). Thus, we subdivided patients according to the increasing expression levels from quartile 1 to 4 of *CDK6-AS1* (Q1, Q2, Q3 (Q123-AML) and Q4, see Figure S1C). *CDK6-AS1* quartile distribution was maintained also subdividing patients according to the genetic abnormalities identified at diagnosis (*p value<0.05, **p value<0.01, see Figure S1D). This latter observation prompted us to investigate the biological role of *CDK6-AS1*. We examined the gene expression profiles (GEPs) of 58 of the 132 patients with AML, of whom 18 had the highest *CDK6-AS1* expression (Q4-AML), whereas 40 belonged to Q123-AML quartiles (GEO: GSE75461). Of note, the unsupervised analysis showed a statistical significant clustering of Q4-AML as compared with the Q123-AML cases, independently of their genetic lesions for 57 coding and 12 ncRNAs with a Fold Change |2| (p value<0.01, coding genes in Figure 1A, for ncRNAs see also Figure S2A) or 247 coding genes and 83 ncRNAs with a Fold Change |1,5| (p value<0.01; see Figure S2B, see Tables S2A and S2B). t-Distributed stochastic neighbor embedding (t-SNE) visualization using the 57 most variably expressed transcripts revealed a clear classification of AML consistent with *CDK6-AS1* expression quartiles (Figure 1B, upper panel). Applying the same method for the different genetic lesions as classifier, we noted that different high-risk genetic lesions, including *FLT3*-ITD, *MLL*-r, *NUP98*-r, and no markers, were present in Q4-AML (Figure 1B, lower panel). We observed that patients with Q4-AML had a greater risk of not achieving complete remission when compared with patients with Q123-AML (Table S1A, p value = 0.03), suggesting a potential role of *CDK6-AS1* in determining patients' response to therapy. The same result was confirmed in another independent cohort of pediatric AML cases (TARGET, n = 110), where high-*CDK6-AS1* patients (Q4) had significantly higher minimal residual disease (MRD) levels after induction therapy with respect to low-*CDK6-AS1* cases (Q123, p value = 0.034; see Table S1B).

Gene Set Enrichment Analysis (GSEA) highlighted that Q4-AML were negatively enriched in genes regulated by the Runt domain of the Runt-related transcription factor 1 (RUNX1), essential for the early hematopoietic differentiation process (Fujimoto et al., 2007). In parallel, a concomitant hyper-expression of genes related to mitochondrial translation processes was found to be upregulated in Q4-AML (Figure 1C).

Among the most differentially expressed genes in Q4-AML, we identified *CDK6-AS1* adjacent gene *CDK6,* located at 7q21.2. Given that lncRNAs are known to transcriptionally regulate other genes *in cis*, we interrogated neighbor genes within a window of 10 Mb, finding a strong expression correlation exclusively between *CDK6* and *CDK6-AS1*, whereas other pairwise correlations were not significant (see Figure S3A). An overall significant positive correlation between *CDK6-AS1* and *CDK6* expression was confirmed in our AML cohort (Figure 1D, Pearson correlation r = 0.7, p value<0.001, see also Figure S3B, *p value<0.05, ****p value<0.0001) not influenced by the presence of recurrent molecular markers (see Figure S3C, Pearson correlation respectively r = 0.79, 0.84, 0.96 and 0.75; p value<0.05). With the goal of further investigating this correlation, we stably knocked down *CDK6-AS1* (*CDK6-AS1* KD) in SHI-1 AML cell line (documented to have high *CDK6-AS1* expression at the same extent of patients with Q4-AML), finding that *CDK6* mRNA transcript and protein levels significantly decreased (Figures 1E and 1F), whereas other neighbor genes (*SAMD9, GATAD1, PEX1, FAM133B)* were not altered (see Figure S3D). These findings indicated that *CDK6-AS1* might coordinate *CDK6* gene expression. Indeed, bioinformatic analysis revealed that the two genes share an overlapping untranslated first exon transcribed in opposite directions, with a

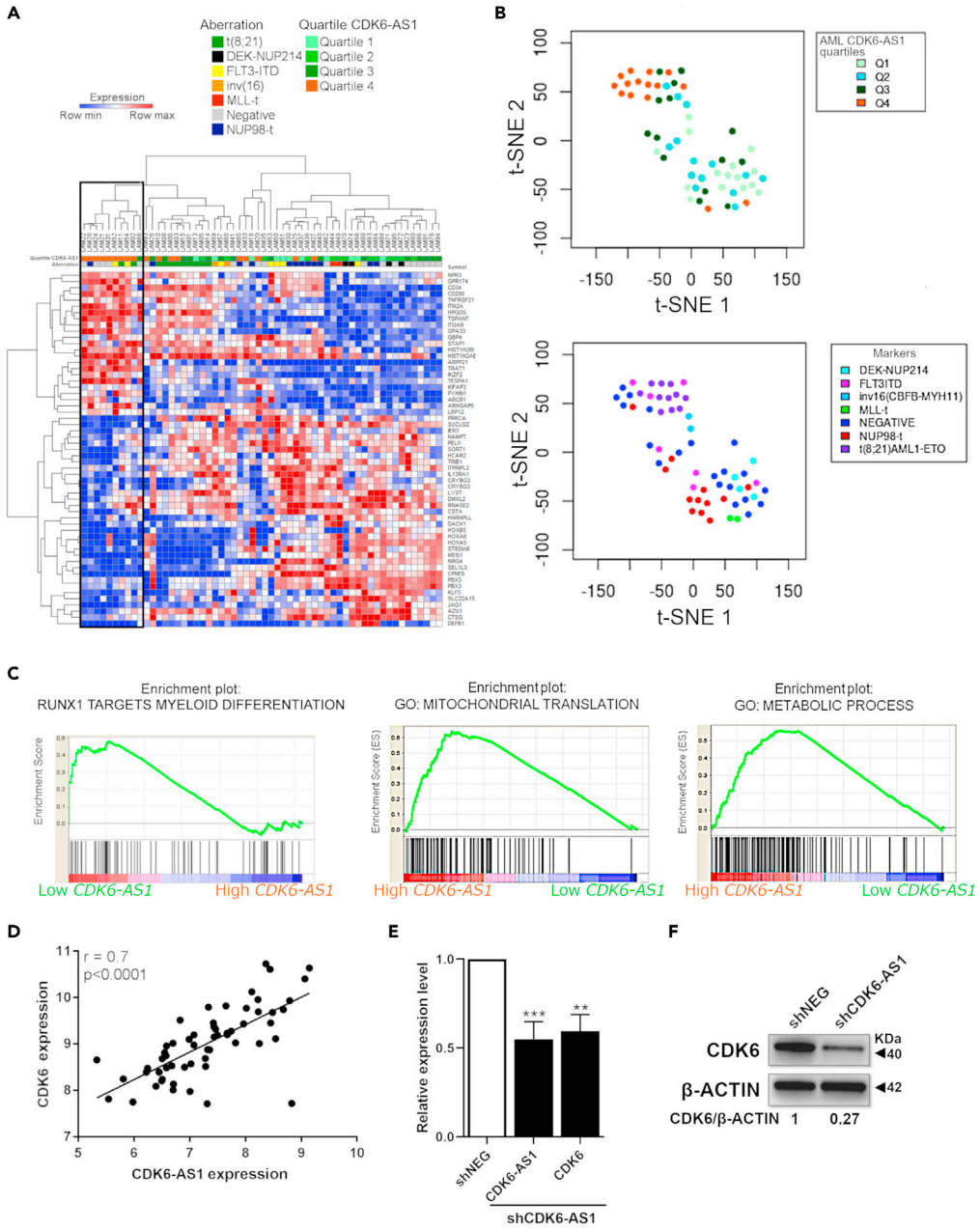

Figure 1. *CDK6-AS1* expression and correlation with *CDK6* in bone marrow samples of pediatric patients with AML

(A) Hierarchical clustering analyses of patients with AML. High-*CDK6-AS1* expression (Q4) patients clustered independently (black square; Pearson correlation distance, t test, p value<0.01, Fold Change FC>|2|) by 57 coding genes (see Table S2A). Genetic AML subtypes and quartile distribution are indicated in the legend with color codes.

(B) t-SNE visualization of patients with AML utilizing the 57 top differentially expressed genes.

(C) Gene Set Enrichment Analysis (GSEA) performed on the 337 gene signature revealed genes of the pathway involved in the upregulation of RUNX1 target genes in patients with Q1-AML *versus* patients with Q4-AML (false discovery rate [FDR] = 0.044, normalized enrichment score (NES) = 1.41) and in mitochondrial synthesis and function being upregulated in the patients with Q4-AML (FDR = 0.0, NES = 2.28 for mitochondrial translation; FDR = 8.12×10^{-5}, NES = 2.17 for metabolic process).

(D) Correlation between *CDK6-AS1* and *CDK6* mRNA expressions (Pearson correlation, r = 0.7, p value<0.0001) plotted in the scatter diagram and fitted in linear regression.

(E) RQ-PCR expression of *CDK6-AS1* and *CDK6* measured in shCDK6-AS1 cells with respect to shRNA NEG (RQ = 1) (n = 4, **p value<0.01, ***p value<0.001). Data are represented as mean ± SEM.

(F) Western blot of CDK6 after stable *CDK6-AS1* silencing with relative densitometric analysis.

promoter region identified by *in silico* analysis for its enrichment in transcription factor binding sites, within exon 1 and intron 1 of *CDK6* (see Figures S4A–S4C). To further corroborate the hypothesis of a common bidirectional promoter for *CDK6-AS1* and *CDK6* controlled by *CDK6-AS1*, we generated a single (only at 3′) and dual (both at 5′ and 3′) luciferase reporter vectors containing 1,400 nucleotides of the predicted promoter. The luciferase expression in transfected cell lines increased using the dual vector with respect to the single luciferase vector, confirming promoter bidirectionality. When we transfected these vectors in *CDK6-AS1* KD we measured a lowered luciferase activity in both constructs, demonstrating that *CDK6-AS1* reduction modulated the promoter in two directions, thus regulating the expression of both CDK6-AS1 and CDK6 (see Figure S4D, *p value<0.05). Consistently, we showed that *CDK6-AS1* was present in both nuclear and cytosolic cell fractions (see Figure S4E, *p value<0.05) and that in the *CDK6-AS1* stable silenced cells its expression levels were decreased both in the nuclear and cytosolic compartments (see Figure S4F, *p value<0.05, **p value<0.01).

CDK6-AS1 correlates with differentiation of hematopoietic progenitors

In order to confirm the contribution of *CDK6-AS1/CDK6* axis in hematopoietic cell differentiation process as suggested by GSEA, we ranked all the transcripts that correlated with *CDK6-AS1* expression in AML cases according to the absolute Spearman's rank correlation coefficient. We used the top 1% probes and identified a 337-transcript signature used to interrogate 33 healthy donor-derived human blood cell samples (GEO: GSE98633) (Schwarzer et al., 2017). By unsupervised clustering we observed that these genes were able to subdivide the healthy immature CD34+ from the myeloid granulocyte-monocyte progenitors (CMP/GMP), and from the more mature hematopoietic pools (granulocytes, erythroblasts, monocytes, and megakaryocytes); this clustering correlates with *CDK6-AS1* expression levels (expressed in quartiles, Figure 2A). t-SNE analysis confirmed that the more immature healthy samples had the highest levels (Q4) of *CDK6-AS1*, whereas more committed populations showed lower *CDK6-AS1* levels (Q123) (Figure 2B, see also Figure S5A, *p value<0.05). These findings highlight that *CDK6-AS1* expression reflects the hematopoietic differentiation stage, in both primary AML samples and healthy hematopoietic cells. At support we investigated *CDK6-AS1* levels in CD34+/CD38- cells from primary AML samples confirming an increased RNA expression in sorted CD34+/CD38- blasts (RQ = *CDK6-AS1* = 1.3, *CDK6* = 5.2) with respect to the rest of blasts (RQ = 1), as well as an increased fluorescence detected by flow cytometry with respect to the non-CD34+/CD38- (see Figure S5B). In line with this observation, we documented an increased percentage of CD34+ cells in samples of patients with AML collected at diagnosis showing higher *CDK6-AS1* expression when compared with AML samples of Q1 for *CDK6-AS1* expression (Figure 2C). To support this observation, we found a higher *CDK6-AS1* and *CDK6* expression (RQ *CDK6-AS1* = 11.9 and RQ *CDK6* = 9.5) in isolated primary normal CD34+ cells when compared with the more mature CD34-counterpart (RQ = 1, Figure 3A, left, *p value<0.05). Finally, we transduced CD34+ cells with sh*CDK6-AS1*, documenting no effects on cell viability (see Figure S5C) but a 20% downregulation of CD34 expression 10 days after silencing (Figure 3A, right, **p value<0.01). On the contrary, we promoted CD34+ cell differentiation by 10-day treatment with ATRA 5μM, documenting that both *CDK6-AS1* and *CDK6* expression decreased (Figure 3B, *p value<0.05, see also Figure S5D). In addition, *CDK6* silencing enhanced CD34+ cell differentiation upon ATRA exposure. By contrast, *CDK6* overexpression delayed CD34+ differentiation (Figure 3C, *p value<0.05, **p value<0.01).

CDK6-AS1/CDK6 axis controls RUNX1 transcriptional program in AML

In line with these results, we explored *CDK6-AS1* role in AML differentiation in AML cell lines. *CDK6-AS1* KD cells acquired CD11b expression, a marker of myeloid maturation with respect to negative control (shNEG) cells (79.5% *versus* 55.2%, respectively, Figure 4A, *p value<0.05; same results were found in transient transfection for HL-60 and U-937 cell lines, see also Figures S6A–S6C, *p value<0.05, **p value<0.01). Functionally, *CDK6-AS1* KD cells showed a significantly increased phagocytic capacity (Figure 4A, right and lower panels, **p value<0.01, see also Figures S6D and S6E, *p value<0.05) that was further augmented when cells were stimulated with GM-CSF (see Figure S6F, *p value<0.05). Moreover, *CDK6-AS1* KD cells showed a reduction of more than 30% in their colony-forming capacity (see Figure S6G, *p value<0.05) and an increase in PU1 protein, a transcription factor implicated in early myeloid differentiation (see Figure S6H), supporting the involvement of *CDK6-AS1* in the block of myeloid differentiation without effects on both cell viability and cell cycle (see Figures S6I and S6J).

Since *CDK6-AS1* depletion in AML cells reduced both CDK6 RNA and protein expression (Figures 1E and 1F), we observed a deregulation in the complex formed by CDK6 with RUNX1, allowing RUNX1 to work as transcription factor, an essential step of the early hematopoietic differentiation process (red spots in Figure 4B, see also Figure S6K) (Fujimoto et al., 2007). We looked at RUNX1 transcriptional program monitoring the 81 RUNX1 target

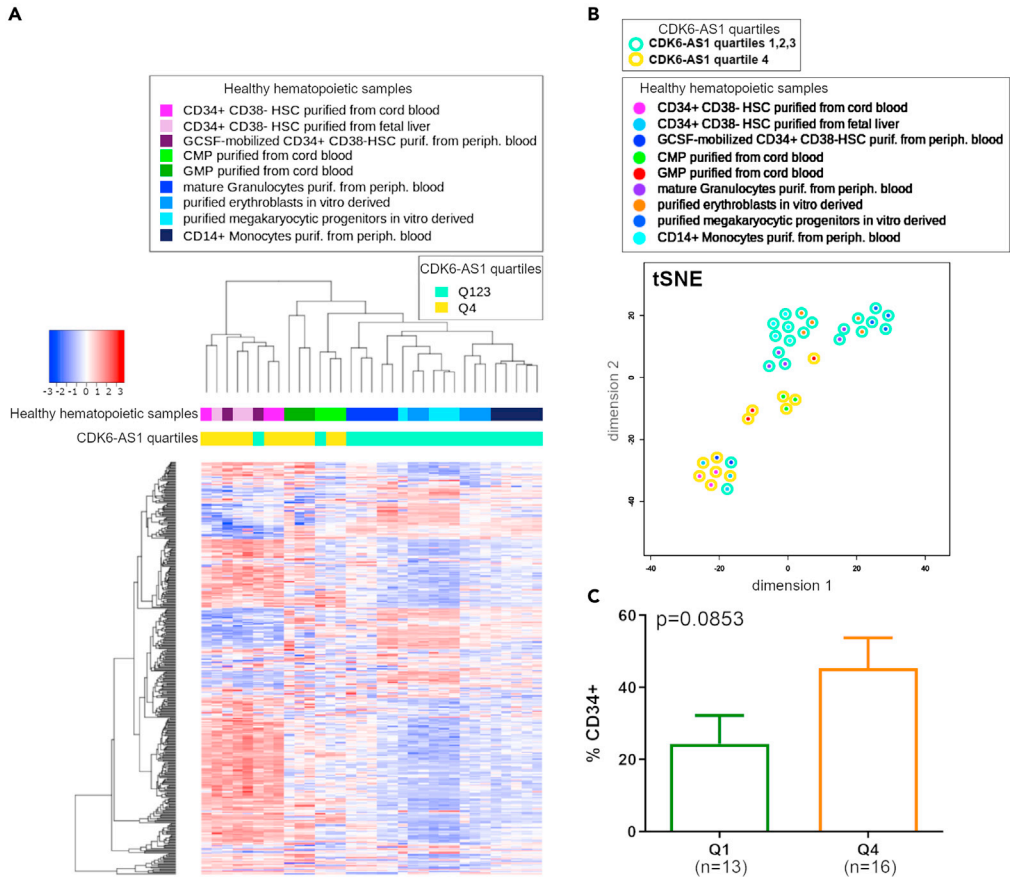

Figure 2. *CDK6-AS1* is associated with a more immature phenotype

(A) Unsupervised hierarchical clustering of healthy hematopoietic samples (GSE98633) (Schwarzer et al., 2017) with the 337-gene signature, subdivided into immature Lin-/CD34+/CD38- of different origins, myeloid monocyte, and granulocyte progenitors (Lin-/CD34+/CD38+/CD123+ CD45RA- CMP and Lin-/CD34+/CD38+/CD123+ CD45RA+ GMP) and more mature hematopoietic cells (CD15+/CD66+ granulocytes, CD36+/GlyA+ erythroblasts, CD14+ monocytes and CD41+/CD42b+ megakaryocytes). Samples were also subdivided into *CDK6-AS1* quartiles.

(B) t-SNE plot of the healthy CD34+, CMP, GMP, and more committed cell pools from healthy donors clustered according to the expression values of the 337-gene signature.

(C) Expression of CD34 antigen in blasts of bone marrow samples of 13 patients with Q1-AML *versus* 16 patients with Q4-AML at diagnosis. Data are represented as mean ± SEM.

genes (deposited in ChEA database [Lachmann et al., 2010] and annotated to myeloid cell differentiation by GO term 0030099) expression in Q1 *versus* Q4-AML cases. Most of the RUNX1 target genes including *PU.1*, *FOS*, *MEIS1*, and *PRDM16* were significantly de-regulated in Q4-AML as shown by PCA, clustering, and GSEA analyses (Figures 1C and 4C, see also Figure S6L, see also Table S3). *Vice versa*, a pro-differentiating effect was obtained by silencing *CDK6* as confirmed by the increased RUNX1 target genes expression, as well as by CD11b/CD16 markers positivity and cell morphology (see Figures S7A–S7D, *p value<0.05, **p value<0.01, ***p value<0.001). Furthermore, the immature phenotype was rescued when we exogenously expressed *CDK6* in *CDK6-AS1* KD cells, as shown by a reduced CD11b expression and phagocytic ability (see Figures S7E–S7G, **p value<0.01). These findings clearly support the hypothesis that aberrant *CDK6-AS1* expression, by controlling *CDK6* levels, triggers the block of early hematopoietic differentiation process, an essential step of the hematopoietic cell transformation.

CDK6-AS1 controls mitochondrial dynamics in AML and healthy CD34+ cells

Since gene expression suggested that differentiation and mitochondrial signatures were related to the *CDK6-AS1* Q4-AML (Figure 1C, right, see also Table S4A) and to healthy hematopoietic cells (see Table S4B), we further investigated this association between hematopoietic differentiation and mitochondrial

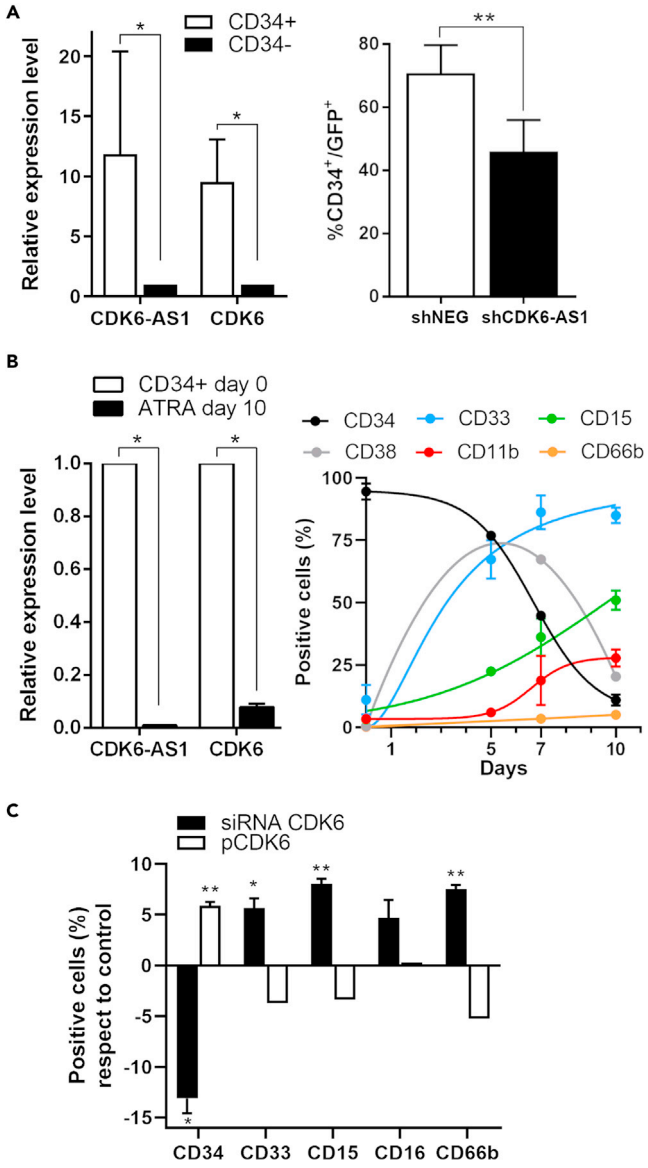

Figure 3. *CDK6-AS1/CDK6* is strongly associated to differentiation in healthy CD34+ cells

(A) *CDK6-AS1* expression in healthy CD34+ and CD34- fractioned population (left, n = 3, *p value<0.05). Decrease in the percentage of CD34+ positive cells upon *CDK6-AS1* depletion (shCDK6-AS1 that are GFP+) evaluated by flow cytometry (right, n = 3, **p value<0.01).

(B) Expression level of *CDK6-AS1* and *CDK6* in normal CD34+ cells at day 0 and after cell differentiation induced by ATRA 5 μM, at day 10 (left, n = 3, *p value<0.05). Expression of several surface markers during ATRA-induced cell differentiation (right).

(C) Percentage of positive cells for several differentiation markers in siRNA CDK6 and pCDK6 transfected healthy CD34+ cells, respect to negative controls siRNA NEG and pØ, respectively, after 7 days with ATRA (5 μM) treatment (n = 2, *p value<0.05, **p value<0.01). Data are represented as mean ± SEM.

dynamics. We examined mitochondrial membrane potential ($\Delta\Psi$) by tetramethylrhodamine, ethyl ester (TMRE) staining in the healthy CD34+ cell population, which was characterized to include several steps of hematopoietic hierarchy (Pellin et al., 2019) (including hematopoietic stem cells CD34+/38-/90+ and other precursor cells, see Figure S8). The $\Delta\Psi$ regulates ATP synthesis, ROS production, calcium homeostasis, import-export of mitochondrial proteins, mitochondrial membrane dynamics for biogenesis, mitochondrial proton conductance, and respiratory chain capacity. We revealed a mitochondrial substructure in CD34+ cells by using $\Delta\Psi$ values: we identified and sorted two different subpopulations, TMRE low and

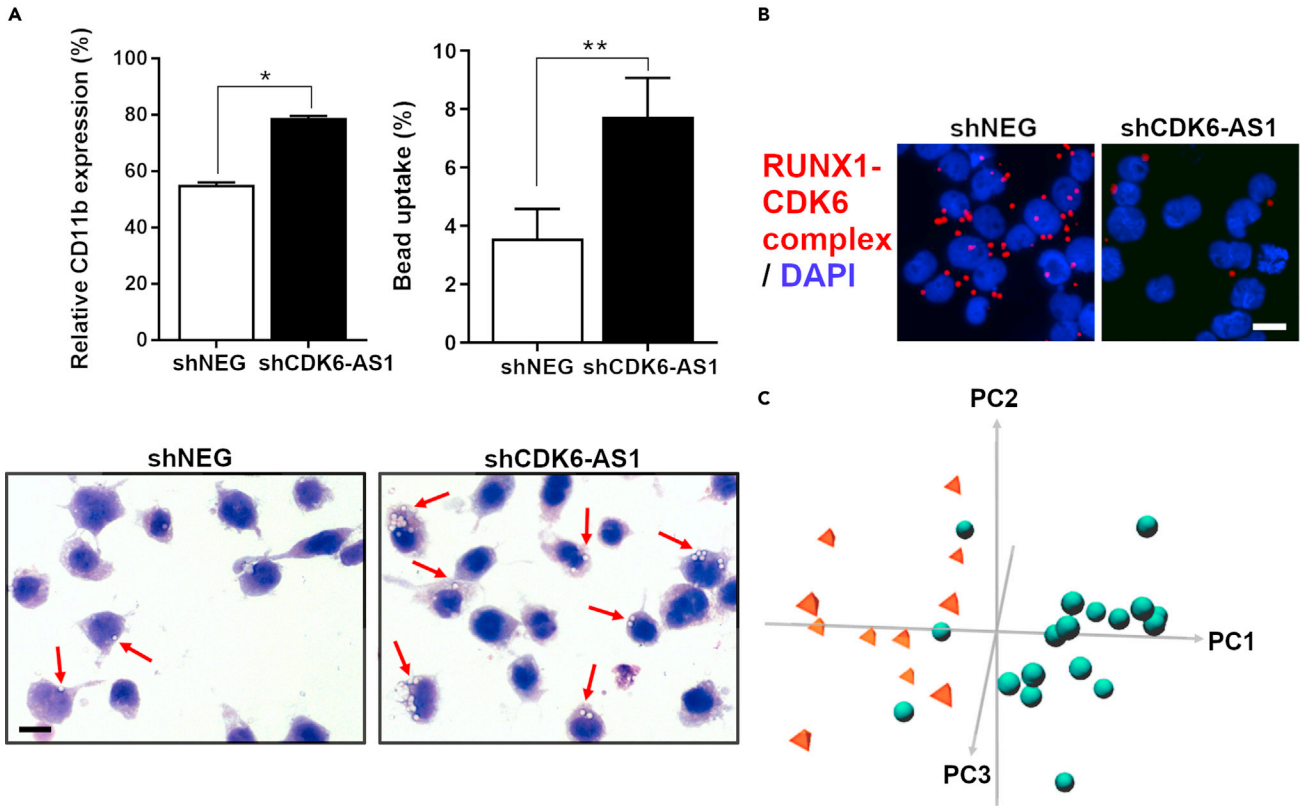

Figure 4. *CDK6-AS1/CDK6* controls hematopoietic differentiation process

(A) CD11b expression in SHI-1 cells after *CDK6-AS1* silencing as compared with control cells (left, n = 3, *p value<0.05). Percentage of bead uptakes in phagocytosis assay (right, n = 4, **p value<0.01) and representative images of phagocytic cells with intracellular beads indicated by arrows, after May-Grünwald Giemsa staining on fibronectin-coated chamber slides (magnification 40x; scale bar, 15 μm). Data are represented as mean ± SEM.

(B) CDK6-RUNX1 complex (red dots) by Proximity Ligation Assay in SHI-1 cells silenced for *CDK6-AS1* expression. Nuclei were stained with DAPI (blue) (40× magnification; scale bar, 15 μm).

(C) Principal component analysis (right panel) of significant *RUNX1* target genes (p value<0.05) involved in myeloid cell differentiation in *CDK6-AS1* Q1-AML (green) *versus* Q4-AML (orange) (FDR q-value <0.25 and p value <0.01).

high, finding that the CD34+/TMRE low were more quiescent, as shown by PyroninY/Hoechst staining, and mainly CD38- with respect to the CD34+/TMRE high counterpart being more proliferating and mostly CD38+ cells (Figure 5A, *p value<0.05, **p value<0.01). Concomitantly, *CDK6-AS1/CDK6* expression is reduced in CD34+/TMRE high after exiting from quiescence to differentiate (RQ = 0.5 for *CDK6-AS1* and RQ = 2.29 for *CDK6*, *versus* CD34+/TMRE low RQ = 1.32 for *CDK6-AS1* and RQ = 14.71 for *CDK6*; Figure 5A, lower panel). These data support the observation that an association between *CDK6-AS1* levels, hematopoietic differentiation, and mitochondrial dynamics exists.

To decipher this latter finding in AML cases, we performed a single-sample GSEA revealing that specific mitochondrial biogenesis signatures were enriched according to *CDK6-AS1* expression (see Figure S9A, *p value<0.05, **p value<0.01, see also Table S4B). Consistently, mitochondrial mass in *CDK6-AS1* KD cells decreased in terms of mitochondrial area (by TOMM20, Figure 5B, left, ****p value<0.0001, see also Figure S9B), mitochondrial DNA content (Lazarou et al., 2015) (see Figure S9C, ****p value<0.0001), and $\Delta\Psi$ (Figure 5B, lower right, *p value<0.05), which was not observed upon *CDK6* silencing (see Figures S9D–S9F). Furthermore, we analyzed the more immature CD34+ cells isolated from patients with bone marrow-derived primary AML at diagnosis and counted a significantly higher number of mitochondria and a 2.5-fold increased $\Delta\Psi$ with respect to the more differentiated CD34- blasts (Figure 5C, *p value<0.05, ****p value<0.0001). This latter finding reflects the hypothesis that AML-CD34+ had higher *CDK6-AS1* levels and mitochondria content than the more differentiated CD34- AML blasts (fold change 2.03, black line inside the histogram in Figure 5C). Altogether, these data confirm that *CDK6-AS1* overexpression

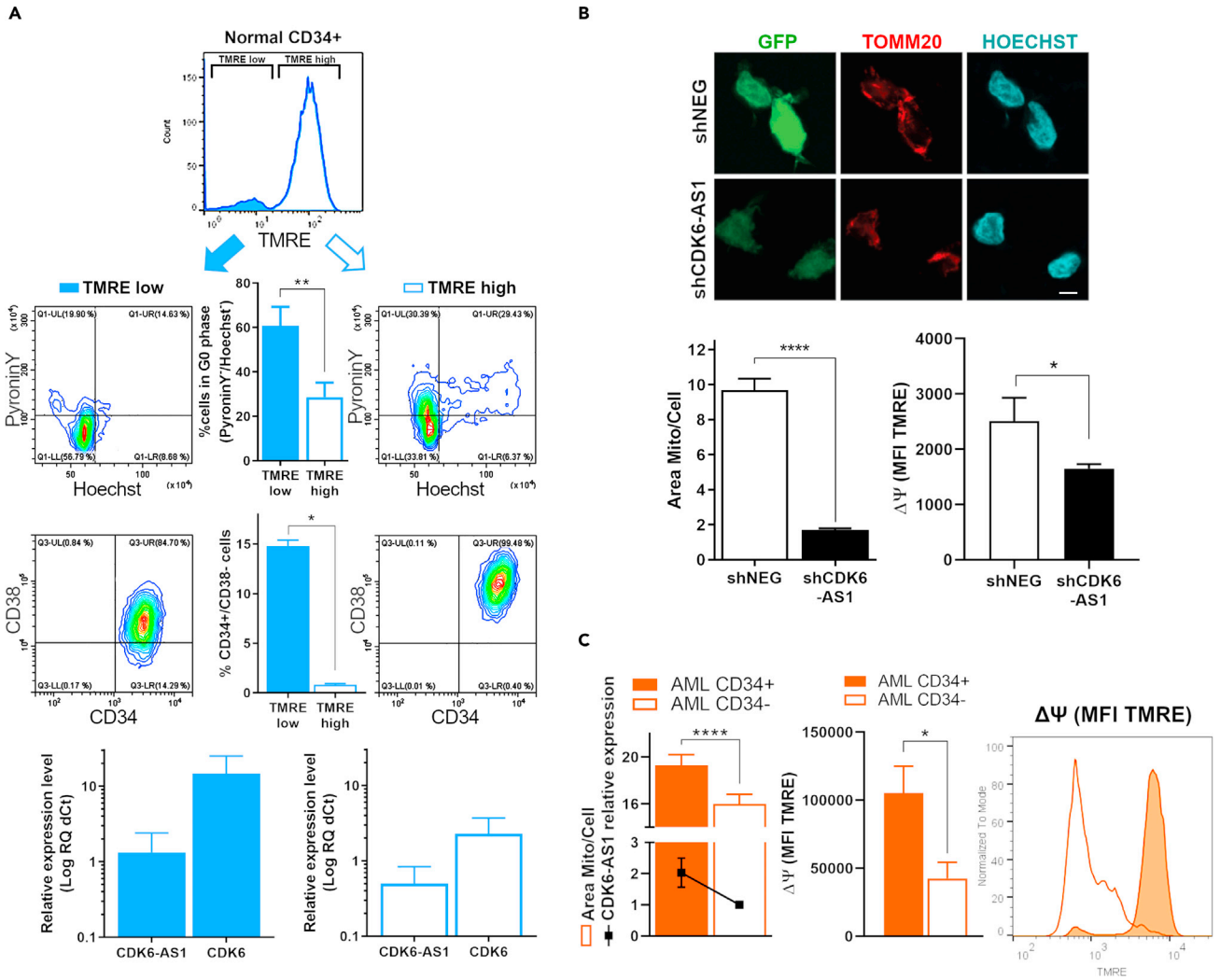

Figure 5. *CDK6-AS1* expression and mitochondrial status in healthy CD34+ and AML cells

(A) Normal CD34+ cells sorted for TMRE expression (TMRE low *versus* TMRE high), analyzed for cell quiescence (cells in G0 phase, negative for Pyronin Y/Hoechst 33342), percentage of CD34+/38- expression, and *CDK6-AS1/CDK6* mRNA level (n = 3, *p value<0.05, **p value<0.01).

(B) Immunostaining of shCDK6-AS1-transduced GFP^{+} (green) SHI-1 cells as compared with control (shNEG), stained for TOMM20 (red). Nuclei staining with Hoechst (blue) (40× magnification; scale bar, 10 μm, upper panel). Mitochondrial mass quantification by TOMM20 (covered area per cell, lower left panel) and mitochondrial membrane potential (**ΔΨ**, fluorescent TMRE probes in flow cytometry, lower right panel) measured in shNEG and shCDK6-AS1 SHI-1 cells (n = 3, *p value<0.05, ****p value<0.0001). Data are represented as mean ± SEM.

(C) Quantification of mitochondrial mass in AML CD34+ and CD34- cells by TOMM20 (orange bars) and *CDK6-AS1* expression level by RQ-PCR in AML-CD34+ with respect to CD34- (RQ = 1) cells (black line into histograms, left). Mitochondrial membrane potential (**ΔΨ**, TMRE staining, right) in AML CD34+ *versus* CD34- cells (n = 3, *p value<0.05, ****p value<0.0001). Data are represented as mean ± SEM.

positively correlates with mitochondrial biogenesis signatures and mass in leukemia cells, and particularly in the CD34+ cell compartment.

These findings supported the idea that *CDK6-AS1* aberrant hyper-expression maintains blasts, including the more immature CD34+ subpopulation, to meet the challenges of high energy demand and promotes drug resistance to evade apoptosis (Lapalombella, 2017; Yoshida, 2015), suggesting that approaches targeting mitochondrial dependencies (Roth et al., 2019) should impact particularly on the *CDK6-AS1* Q4-AML cases. We confirmed that three of the tested compounds targeting mitochondria processes, Tigecycline (TIGE, mitochondrial translation inhibitor), Oligomycin (OLIG, mitochondrial complex V inhibitor), and Rotenone (ROT, mitochondrial complex I inhibitor), were more effective in reducing viability in *CDK6-AS1* KD cells. On the other hand, Venetoclax (VEN, anti-apoptotic mitochondrial proteins),

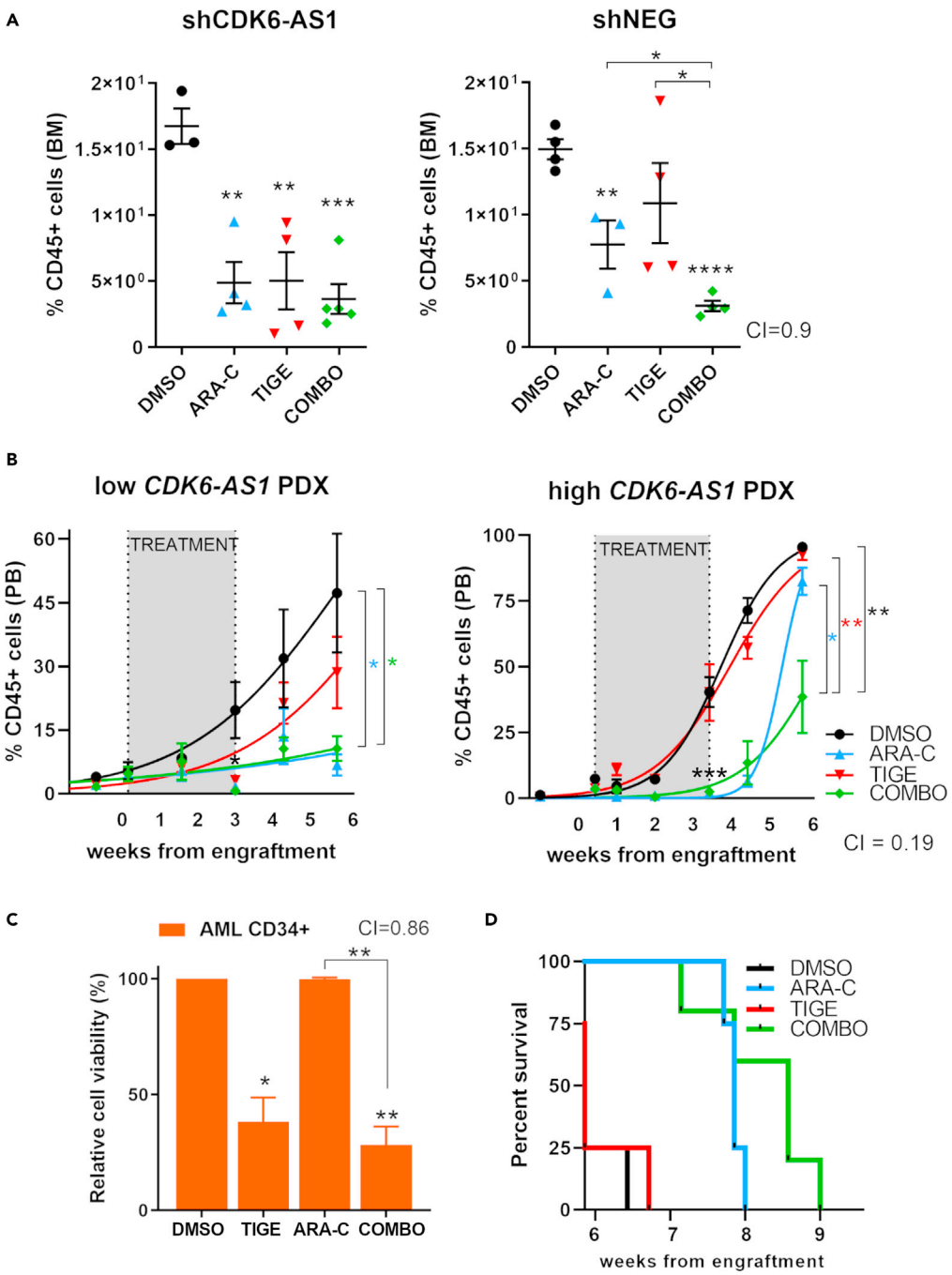

Figure 6. TIGE sensitization to chemotherapy in high-*CDK6-AS1* AML

(A) Detection of hCD45+ AML cells in bone marrow (BM) of NSG mice inoculated with shCDK6-AS1 SHI-1 cell line (low-*CDK6-AS1* AML mice, left) or shNEG SHI-1 cell line (high-*CDK6-AS1* AML mice, right), after 2-week treatment with TIGE 75 mg/kg or ARA-C 25 mg/kg and combination therapy (COMBO). Synergistic effect in shNEG (Combination Index CI = 0.9; mice n = 3/5 per group, *p value<0.05, **p value<0.01, ***p value<0.001, ****p value<0.0001). Data are represented as mean ± SEM.

(B) Percentage of hCD45+ AML cells detected in peripheral blood (PB) of low- (left) and high- (right) *CDK6-AS1* PDXs with TIGE, ARA-C, or COMBO (after 3-week treatment *p value<0.05, ***p value<0.001 of treated mice with respect to DMSO). Monitoring of hCD45 during 3 weeks after treatment discontinuation (mice n = 4/5 per group; *p value<0.05, **p value<0.01). Synergistic effect of COMBO in high-*CDK6-AS1* PDX (CI = 0.19).

Figure 6. *Continued*

(C) *In vitro* cell viability after 24-h treatment with TIGE, ARA-C, or COMBO in AML patient-derived CD34+ cells. Combination index CI = 0.86 (n = 2, *p value<0.05, **p value<0.01). Data are represented as mean ± SEM.

(D) Overall survival Kaplan-Meier analysis. Median survival in days from end of treatment: DMSO 19.5, TIGE 20, ARA-C 34, COMBO 39 (log rank Mantel-Cox test: p value DMSO *versus* ARA-C = 0.0062 **, DMSO *versus* TIGE = ns, TIGE *versus* ARA-C = 0.0069 **, DMSO *versus* COMBO = 0.0025 **, COMBO *versus* TIGE = 0.0029 **).

Enasidenib (ENA, anti-mitochondrial IDH-2 drug), and Ivosidenib (IVO, anti-cytoplasmic IDH-1 drug) did not show differential efficacy in *CDK6-AS1* KD with respect to control cells (see Figure S10, **p value<0.01, ***p value<0.001, ****p value<0.0001) probably because they are indirectly targeting mitochondria.

Mitochondrial targeting sensitizes high *CDK6-AS1* AML to chemotherapy

Since TIGE was previously reported to produce preclinical results against AML (Jin et al., 2019; Škrtić et al., 2011), we focused on this compound and tested its potency as an anti-mitochondrial agent. AML cells with low (shCDK6-AS1) and high (shNEG) *CDK6-AS1* expression were inoculated in NSG mice and treated with low-dose Cytarabine (25 mg/kg ARA-C) (Wunderlich et al., 2013), TIGE (75 mg/kg), and a combination strategy (ARA-C + TIGE, COMBO). We found that all treatments mediate the same leukemia reduction in shCDK6-AS1 mice (having reduced mitochondria, Figure 6A, left, **p value<0.01, ***p value<0.001), whereas the COMBO treatment decreased the percentage of CD45+ AML cells with high *CDK6-AS1* levels (shNEG) when compared with ARA-C and TIGE treatment alone (Figure 6A, right, *p value<0.05, **p value<0.01, ****p value<0.0001; Synergistic Combination Index<1, CI = 0.9; confirmed by spleen length, see Figure S11A, **p value<0.01, ****p value<0.0001). Then, we moved to primary AML samples previously studied for *CDK6-AS1* expression levels and mitochondrial mass (see Figures S11B and S11C, ****p value<0.0001). We found that primary AML samples with low *CDK6-AS1* were sensitive to all treatments, and COMBO treatment was the most effective treatment in reducing high *CDK6-AS1* blasts viability (see Figure S11D, *p value<0.05, **p value<0.01, ****p value<0.0001, CI = 0.85 for high-*CDK6-AS1* patient). *In vivo*, after engraftment, low- and high-*CDK6-AS1* patient-derived xenografts (PDXs) were treated for 3 weeks showing that ARA-C and COMBO strategies were effective in reaching AML remission (Figure 6B, gray area, *p value<0.05, ***p value<0.001). After treatment discontinuation both models relapsed, but faster in the high-*CDK6-AS1* PDX animals treated with ARA-C alone with respect to the COMBO that delayed leukemia progression thanks to mito-mass targeting (Figure 6B, right, *p value<0.05, **p value<0.01, CI = 0.19). Moreover, in CD34+ cells sorted from primary AML samples mitochondrial targeting was effective and synergistically active *in vitro* when combined with ARA-C (Figure 6C, *p value<0.05, **p value<0.01, CI = 0.86). Finally, we observed that mice with high-*CDK6-AS1* AML treated with COMBO benefited from a prolonged survival (Figure 6D). These results provide the rationale for further considering the *CDK6-AS1* levels as a marker in defining those AML cases that could benefit from combined mitochondrial-targeting therapies to prevent leukemia progression.

DISCUSSION

Front-line therapy in most cancer is still mainly based on the use of chemotherapy, but, in many patients, drug resistance and persistent disease after treatment discontinuation result in tumor recurrence and poor outcome (Pession et al., 2013; Ramos et al., 2015). Our study was designed with the goal of discovering markers able to improve stratification of pediatric patients with AML, with great interest toward the non-coding transcriptome, shown to cluster pediatric AML with the same accuracy as protein coding genes and found to have the potential to dissect unexplored AML networks (Deveson et al., 2017; Schwarzer et al., 2017; Zampini et al., 2017). In this study, we identified that the lncRNA *CDK6-AS1*, together with its neighbor gene *CDK6* (Lai et al., 2013), is a robust marker of a specific AML subgroup with features similar to those found in healthy CD34+ cells, including an early myeloid differentiation arrest and enhanced mitochondria biogenesis. Functionally, *CDK6-AS1* depletion increased differentiation of CD34+ cells, this finding being consistent with the idea that *CDK6-AS1* is important in regulating the balance between differentiation potential and self-renewal capacity in both normal and leukemic cells. Indeed, we produced data showing that. at the first stages of CD34+ differentiation, the more quiescent CD38- cells expressed higher *CDK6-AS1/CDK6* levels, which decrease when differentiation occurs in CD38+ cells. This observation highlights that *CDK6-AS1* is important in the characterization of early *versus* late progenitors, including CD34+ *versus* CD34- hematopoietic cells of both healthy and AML subjects. This finding supports the concept that aberrant *CDK6-AS1/CDK6* expression during hematopoietic commitment could provide a key transforming event inducing the block of myeloid differentiation (Schmoellerl et al., 2020). In the AML context, we found a clue as to how this might occur: *CDK6-AS1*, being hyper-expressed, modulates

CDK6 levels and CDK6-RUNX1 interaction, inhibiting several RUNX1 promoters (Fujimoto et al., 2007) with decreased expression of differentiation factors, including *PU.1*, *MEIS1*, and *RUNX1* itself. In line with these findings, reduced *CDK6-AS1/CDK6* expression in AML led to the emergence of more differentiated cells with reduced *in vitro* clonogenic potential. This confirms *CDK6-AS1/CDK6* axis playing a role in the hematopoietic differentiation program, suggesting that *CDK6-AS1* aberrant hyper-expression might concur during the leukemogenesis process (Corrà et al., 2018; Laurenti et al., 2015; Schwarzer et al., 2017).

In addition, we found an association between high *CDK6-AS1* levels and mitochondrial biogenesis pathway activation. Sorting healthy CD34+ cells according to their mitochondrial membrane potential, we confirmed that *CDK6-AS1* levels decreased along the hematopoietic differentiation process together with the concomitant mitochondrial biogenesis targets activation (Anderson et al., 2018; Ploumi et al., 2017; Škrtić et al., 2011; Vo et al., 2012). It is well known that cancer cells modulate metabolic programs toward a complex balance of satisfying demands for macromolecular synthesis, energy production, and resistance to cell stress and drugs, supporting tumor aggressiveness (Roth et al., 2019; Yoshida, 2015). Our data suggest that high *CDK6-AS1* levels exert a transcriptional control to enhance mitochondrial mass in leukemia cells. Indeed, when we decreased *CDK6-AS1* levels in AML blasts, their mitochondrial status was altered, with a severely reduced mitochondrial mass and membrane potential, suggesting a putatively modified chemotherapy susceptibility (Soderquist et al., 2018; Vo et al., 2012; Zhao et al., 2019), as documented by previous data indicating that the mitochondrial number is tightly regulated to maintain pathophysiological cellular activity (Kuntz et al., 2017; Škrtić et al., 2011) or to reduce drug sensitivity in cancer (Chen et al., 2019; Soderquist et al., 2018). Interestingly, *CDK6-AS1* was previously shown to regulate glucocorticoid chemosensitivity in B-ALL blasts (Fernando et al., 2015), and we speculated that this mechanism may be involved also in AML. In fact, recently, mitochondrial-targeted therapies were successfully used in preclinical studies demonstrating IDH-targeted therapy and BCL-2 inhibitors, like Venetoclax, being active in adult AML (Chen et al., 2019; Sarosiek et al., 2013; Waitkus et al., 2018). Thus, to support a mitochondrial-oriented approach for a specific pediatric AML subgroup, we tested whether chemotherapy-induced cytotoxicity and mitochondrial targeting can synergistically improve the killing of those AML cells with the highest *CDK6-AS1* (Q4-AML), including the CD34+/CD38- AML subpopulation. Collectively, our *in vitro* and *in vivo* studies revealed a clear pattern of increased AML cell vulnerability for the majority of mitochondrial drugs used as single agent when *CDK6-AS1* was silenced, implying the possibility to identify selective drugs for different AML subsets. Furthermore, since *CDK6-AS1* levels correlated with mitochondrial mass, we assigned it the role of an AML determinant of drug sensitivity. The dynamic *CDK6-AS1* expression range, associated with mitochondrial status, could allow the identification of those patients who can benefit from a mitochondrial targeting combined with chemotherapy, as we demonstrated by combining TIGE with ARA-C. The applicability of our approach has been validated in a pilot *in vivo* AML-PDX model with high *CDK6-AS1* levels. The most striking finding of this experiment is that the use of an antibiotic inhibiting mitochondrial protein translation was synergistic with ARA-C (Jin et al., 2019), impacting on AML progression, suggesting that *CDK6-AS1* might guide for mitochondrial drugs approaches in further pre-clinical settings.

To the best of our knowledge, this is the first work that demonstrates the potency of a lncRNA in controlling an axis that regulates mitochondrial homeostasis and, in concert with its neighbor gene *CDK6*, the myeloid differentiation process. Our findings indicate that the measurement of a single lncRNA at diagnosis might orient clinicians to specific therapeutic strategies. Further studies aimed at investigating the efficacy of mitochondrial drugs, either alone or in combination with conventional chemotherapy, will be instrumental to further corroborate our data and to pursue novel strategies able to reduce relapse occurrence in children with high risk of relapse in AML.

Limitations of the study

Since this study is based on retrospective analyses, the potential bias from different cohorts of patients is inevitable. The investigation of the *CDK6-AS1* expression profile and the validation of its role in resistance to therapy in a larger population is recommended. Furthermore, additional efforts should be performed to deeply analyze the *CDK6-AS1* mechanism in leukemia. Moreover, our findings encourage the use of other anti-mitochondrial agents to significantly improve AML sensitivity to standard chemotherapy.

STAR★METHODS

Detailed methods are provided in the online version of this paper and include the following:

- KEY RESOURCES TABLE

SUPPLEMENTAL INFORMATION

Supplemental information can be found online at https://doi.org/10.1016/j.isci.2021.103350.

ACKNOWLEDGMENTS

The authors are grateful to Roberta Destro, Matteo Borioni, and Barbara Sartini of the Cord Blood Bank of the Oncology/Hematology Clinic in Padova. We thank the staff of the Oncology/Hematology laboratory for the diagnostic characterization of AML samples. In particular, we would like to express our gratitude to Katia Polato, Barbara Buldini, and Anna Leslz of the Biobanca Oncologia Pediatrica (BBOP). We thank Vito Barbieri for technical support in the mice facility.

This article is in loving memory of Prof. Giuseppe Basso.

This work was supported by grants to M.P. from Università degli Studi di Padova, CARIPARO grant 17/04, AIL-PD and AIL-TV, AIRC IG 2017-ID20562 and CoG-21/06 Pediatric Research Institute (IRP); AIRC (Special Grant "5xmille"-9962 to F.L.); by Ministero della Salute (RF-2010-2316606) to F.L.

AUTHOR CONTRIBUTIONS

Conceptualization, M.P., E.P., M. Benetton, V.B.; methodology, A.D.R., E.P., V.B., M. Benetton; formal analysis, C.Z., E.P., M. Benetton, V.B.; investigation, E.P., M. Benetton, V.B., G.B., A.D.R., C.T., G.G., M. Bordi, S.C.; resources, M.P., F.L., D.S.R., S.M.; writing – original draft, M.P., E.P., M. Benetton, V.B., D.S.R., F.L.; writing – review & editing, M.P., E.P., M. Benetton; supervision, M.P.; funding acquisition, M.P., F.L.

DECLARATION OF INTERESTS

D.S.R. is an inventor on a patent, assigned to UCLA, relating to "Methods and compositions involving lincRNA and leukemia; all other co-authors declare no competing financial and non-financial interests.

Received: July 1, 2021
Revised: September 30, 2021
Accepted: October 22, 2021
Published: November 19, 2021

REFERENCES

Anderson, G.R., Wardell, S.E., Cakir, M., Yip, C., Ahn, Y.R., Ali, M., Yllanes, A.P., Chao, C.A., McDonnell, D.P., and Wood, K.C. (2018). Dysregulation of mitochondrial dynamics proteins are a targetable feature of human tumors. Nat. Commun. *9*, 1677.

Bacher, U., Dicker, F., Haferlach, C., Alpermann, T., Rose, D., Kern, W., Haferlach, T., and Schnittger, S. (2014). Quantification of rare NPM1 mutation subtypes by digital PCR. Br. J. Haematol. *167*, 710–714.

Bester, A.C., Lee, J.D., Chavez, A., Lee, Y.R., Nachmani, D., Vora, S., Victor, J., Sauvageau, M., Monteleone, E., Rinn, J.L., et al. (2018). An integrated genome-wide CRISPRa approach to functionalize lncRNAs in drug resistance. Cell *173*, 649–664.e20.

Bisio, V., Zampini, M., Tregnago, C., Manara, E., Salsi, V., Di Meglio, A., Masetti, R., Togni, M., Di Giacomo, D., Minuzzo, S., et al. (2017). NUP98-fusion transcripts characterize different biological entities within acute myeloid leukemia: a report from the AIEOP-AML group. Leukemia *31*, 974–977.

Bolouri, H., Farrar, J.E., Triche, T., Ries, R.E., Lim, E.L., Alonzo, T.a., Ma, Y., Moore, R., Mungall, A.J., Marra, M.a., et al. (2018). The molecular landscape of pediatric acute myeloid leukemia reveals recurrent structural alterations and age-specific mutational interactions. Nat. Med. *24*, 103–112.

Buldini, B., Rizzati, F., Masetti, R., Fagioli, F., Menna, G., Micalizzi, C., Putti, M.C., Rizzari, C., Santoro, N., Zecca, M., et al. (2017). Prognostic significance of flow-cytometry evaluation of minimal residual disease in children with acute myeloid leukaemia treated according to the AIEOP-AML 2002/01 study protocol. Br. J. Haematol. *177*, 116–126.

Chen, X., Glytsou, C., Zhou, H., Narang, S., Reyna, D.E., Lopez, A., Sakellaropoulos, T., Gong, Y., Kloetgen, A., Yap, Y.S., et al. (2019). Targeting mitochondrial structure sensitizes acute myeloid leukemia to Venetoclax treatment. Cancer Discov. *9*, 890–909.

Corrà, F., Agnoletto, C., Minotti, L., Baldassari, F., and Volinia, S. (2018). The network of non-coding RNAs in cancer drug resistance. Front. Oncol. *8*, 327.

Deveson, I.W., Hardwick, S.A., Mercer, T.R., and Mattick, J.S. (2017). The dimensions, dynamics, and relevance of the mammalian noncoding transcriptome. Trends Genet. *33*, 464–478.

Dykes, I.M., and Emanueli, C. (2017). Transcriptional and post-transcriptional gene regulation by long non-coding RNA. Genomics, Proteomics Bioinforma *15*, 177–186.

Fernando, T.R., Rodriguez-Malave, N.I., Waters, E.V., Yan, W., Casero, D., Basso, G., Pigazzi, M., and Rao, D.S. (2015). LncRNA expression discriminates karyotype and predicts survival in B-lymphoblastic leukemia. Mol. Cancer Res. *13*, 839–851.

Foucquier, J., and Guedj, M. (2015). Analysis of drug combinations: current methodological landscape. Pharmacol. Res. Perspect. *3*, e00149.

Fujimoto, T., Anderson, K., Jacobsen, S.E.W., Nishikawa, S.I., and Nerlov, C. (2007). Cdk6 blocks myeloid differentiation by interfering with Runx1 DNA binding and Runx1-C/EBPα interaction. EMBO J. *26*, 2361–2370.

Inaba, H., Coustan-Smith, E., Cao, X., Pounds, S.B., Shurtleff, S.A., Wang, K.Y., Raimondi, S.C., Onciu, M., Jacobsen, J., Ribeiro, R.C., et al. (2012). Comparative analysis of different approaches to measure treatment response in acute myeloid leukemia. J. Clin. Oncol. *30*, 3625–3632.

Jin, J., Tong, H., and Haiyang, Y. (2019). Combination of tigecycline and Homoharringtonine synergistically enhances anti-leukemia and anti-MDS effect Followed by inhibiting mitochondrial translation through AKT/Mtorpathway and downregulation of anti-apoptotic proteins. Blood *134*, 5387.

Jongen-Lavrencic, M., Grob, T., Hanekamp, D., Kavelaars, F.G., al Hinai, A., Zeilemaker, A., Erpelinck-Verschueren, C.A.J., Gradowska, P.L., Meijer, R., Cloos, J., et al. (2018). Molecular minimal residual disease in acute myeloid leukemia. N. Engl. J. Med. *378*, 1189–1199.

Kuntz, E.M., Baquero, P., Michie, A.M., Dunn, K., Tardito, S., Holyoake, T.L., Helgason, G.V., and Gottlieb, E. (2017). Targeting mitochondrial oxidative phosphorylation eradicates therapy-resistant chronic myeloid leukemia stem cells. Nat. Med. *23*, 1234–1240.

Lachmann, A., Xu, H., Krishnan, J., Berger, S.I., Mazloom, A.R., and Ma'ayan, A. (2010). ChEA: transcription factor regulation inferred from integrating genome-wide ChIP-X experiments. Bioinformatics *26*, 2438–2444.

Lai, F., Orom, U.A., Cesaroni, M., Beringer, M., Taatjes, D.J., Blobel, G.A., and Shiekhattar, R. (2013). Activating RNAs associate with Mediator to enhance chromatin architecture and transcription. Nature *494*, 497–501.

Lapalombella, R. (2017). Mitochondria on the move: BMSCs fuel AML energy. Blood *130*, 1603–1604.

Laurenti, E., Frelin, C., Xie, S., Ferrari, R., Dunant, C.F.F., Zandi, S., Neumann, A., Plumb, I., Doulatov, S., Chen, J., et al. (2015). CDK6 levels regulate quiescence exit in human hematopoietic stem cells. Cell Stem Cell *16*, 302–313.

Lazarou, M., Sliter, D.A., Kane, L.A., Sarraf, S.A., Wang, C., Burman, J.L., Sideris, D.P., Fogel, A.I., and Youle, R.J. (2015). The ubiquitin kinase PINK1 recruits autophagy receptors to induce mitophagy. Nature *524*, 309–314.

Luo, Y., Liang, M., Yao, W., Liu, J., Niu, Q., Chen, J., Liu, Z., Li, M., Shi, B., Pan, J., et al. (2018). Functional role of lncRNA LOC101927497 in N-methyl-N′-nitro-N-nitrosoguanidine-induced malignantly transformed human gastric epithelial cells. Life Sci. *193*, 93–103.

Manara, E., Baron, E., Tregnago, C., Aveic, S., Bisio, V., Bresolin, S., Masetti, R., Locatelli, F., Basso, G., and Pigazzi, M. (2014). MLL-AF6 fusion oncogene sequesters AF6 into the nucleus to trigger RAS activation in myeloid leukemia. Blood *124*, 263–272.

Masetti, R., Pigazzi, M., Togni, M., Astolfi, A., Indio, V., Manara, E., Casadio, R., Pession, A., Basso, G., and Locatelli, F. (2013). CBFA2T3-GLIS2 fusion transcript is a novel common feature in pediatric, cytogenetically normal AML, not restricted to FAB M7 subtype. Blood *121*, 3469–3472.

McKeown, M.R., Corces, M.R., Eaton, M.L., Fiore, C., Lee, E., Lopez, J.T., Chen, M.W., Smith, D., Chan, S.M., Koenig, J.L., et al. (2017). Superenhancer analysis defines novel epigenomic subtypes of non-APL AML, including an RARα dependency targetable by SY-1425, a potent and selective RARα agonist. Cancer Discov. *7*, 1136–1153.

McNeer, N.A., Philip, J., Geiger, H., Ries, R.E., Lavallée, V.P., Walsh, M., Shah, M., Arora, K., Emde, A.K., Robine, N., et al. (2019). Genetic mechanisms of primary chemotherapy resistance in pediatric acute myeloid leukemia. Leukemia. https://doi.org/10.1038/s41375-019-0402-3.

Ng, S.W.K., Mitchell, A., Kennedy, J.A., Chen, W.C., McLeod, J., Ibrahimova, N., Arruda, A., Popescu, A., Gupta, V., Schimmer, A.D., et al. (2016). A 17-gene stemness score for rapid determination of risk in acute leukaemia. Nature *540*, 433–437.

Ng, P.K.S., Li, J., Jeong, K.J., Shao, S., Chen, H., Tsang, Y.H., Sengupta, S., Wang, Z., Bhavana, V.H., Tran, R., et al. (2018). Systematic functional annotation of somatic mutations in cancer. Cancer Cell *33*, 450–462.e10.

Papaemmanuil, E., Gerstung, M., Bullinger, L., Gaidzik, V.I., Paschka, P., Roberts, N.D., Potter, N.E., Heuser, M., Thol, F., Bolli, N., et al. (2016). Genomic classification and prognosis in acute myeloid leukemia. N. Engl. J. Med. *374*, 2209.

Pellin, D., Loperfido, M., Baricordi, C., Wolock, S.L., Montepeloso, A., Weinberg, O.K., Biffi, A., Klein, A.M., and Biasco, L. (2019). A comprehensive single cell transcriptional landscape of human hematopoietic progenitors. Nat. Commun. *10*, 2395.

Pession, A., Masetti, R., Rizzari, C., Putti, M.C., Casale, F., Fagioli, F., Luciani, M., Lo Nigro, L.,

Menna, G., Micalizzi, C., et al. (2013). Results of the AIEOP AML 2002/01 multicenter prospective trial for the treatment of children with acute myeloid leukemia. Blood *122*, 170–178.

Pigazzi, M., Manara, E., Baron, E., and Basso, G. (2008). ICER expression inhibits leukemia phenotype and controls tumor progression. Leukemia *22*, 2217–2225.

Pigazzi, M., Masetti, R., Bresolin, S., Beghin, A., Di Meglio, A., Gelain, S., Trentin, L., Baron, E., Giordan, M., Zangrando, A., et al. (2011). MLL partner genes drive distinct gene expression profiles and genomic alterations in pediatric acute myeloid leukemia: an AIEOP study. Leukemia *25*, 560–563.

Pigazzi, M., Manara, E., Bisio, V., Aveic, S., Masetti, R., Menna, G., Zecca, M., Pession, A., Locatelli, F., and Basso, G. (2012). Screening of novel genetic aberrations in pediatric acute myeloid leukemia: a report from the AIEOP AML-2002 study group. Blood *120*, 3860–3862.

Pigazzi, M., Manara, E., Buldini, B., Beqiri, V., Bisio, V., Tregnago, C., Rondelli, R., Masetti, R., Caterina Putti, M., Fagioli, F., et al. (2015). Minimal residual disease monitored after induction therapy by rq-pcr can contribute to tailor treatment of patients with t(8;21) runx1-runx1t1 rearrangement. Haematologica *100*, e99–e101.

Ploumi, C., Daskalaki, I., and Tavernarakis, N. (2017). Mitochondrial biogenesis and clearance: a balancing act. FEBS J. *284*, 183–195.

Quinn, J.J., Zhang, Q.C., Georgiev, P., Ilik, I.A., Akhtar, A., and Chang, H.Y. (2016). Rapid evolutionary turnover underlies conserved lncRNA-genome interactions. Genes Dev. *30*, 191–207.

Ramos, N., Mo, C., Karp, J., and Hourigan, C. (2015). Current approaches in the treatment of relapsed and refractory acute myeloid leukemia. J. Clin. Med. *4*, 665–695.

Roth, K.G., Mambetsariev, I., Kulkarni, P., and Salgia, R. (2019). The mitochondrion as an emerging therapeutic target in cancer. Trends Mol. Med. *26* (1), 119–134.

Rubnitz, J.E., Inaba, H., Dahl, G., Ribeiro, R.C., Bowman, W.P., Taub, J., Pounds, S., Razzouk, B.I., Lacayo, N.J., Cao, X., et al. (2010). Minimal residual disease-directed therapy for childhood acute myeloid leukaemia: results of the AML02 multicentre trial. Lancet Oncol. *11*, 543–552.

Salmena, L., Poliseno, L., Tay, Y., Kats, L., and Pandolfi, P.P. (2011). A ceRNA hypothesis: the rosetta stone of a hidden RNA language? Cell *146*, 353–358.

Sarosiek, K.A., Ni Chonghaile, T., and Letai, A. (2013). Mitochondria: gatekeepers of response to chemotherapy. Trends Cell Biol. *23*, 612–619.

Schmitt, A.M., and Chang, H.Y. (2016). Long noncoding RNAs in cancer pathways. Cancer Cell *29*, 452–463.

Schmoellerl, J., Barbosa, I.A.M., Eder, T., Brandstoetter, T., Schmidt, L., Maurer, B., Troester, S., Pham, H.T.T., Sagarajit, M., Ebner, J., et al. (2020). CDK6 is an essential direct target of NUP98 fusion proteins in acute myeloid leukemia. Blood *136*, 387–400.

Schwarzer, A., Emmrich, S., Schmidt, F., Beck, D., Ng, M., Reimer, C., Adams, F.F., Grasedieck, S., Witte, D., Käbler, S., et al. (2017). The non-coding RNA landscape of human hematopoiesis and leukemia. Nat. Commun. *8*, 218.

Škrtić, M., Sriskanthadevan, S., Jhas, B., Gebbia, M., Wang, X., Wang, Z., Hurren, R., Jitkova, Y., Gronda, M., Maclean, N., et al. (2011). Inhibition of mitochondrial translation as a therapeutic strategy for human acute myeloid leukemia. Cancer Cell *20*, 674–688.

Soderquist, R.S., Crawford, L., Liu, E., Lu, M., Agarwal, A., Anderson, G.R., Lin, K.H., Winter, P.S., Cakir, M., and Wood, K.C. (2018). Systematic mapping of BCL-2 gene dependencies in cancer reveals molecular determinants of BH3 mimetic sensitivity. Nat. Commun. *9*, 3513.

Tregnago, C., Manara, E., Zampini, M., Bisio, V., Borga, C., Bresolin, S., Aveic, S., Germano, G., Basso, G., and Pigazzi, M. (2016). CREB engages C/EBPδ to initiate leukemogenesis. Leukemia *30*, 1887–1896.

Tregnago, C., Da Ros, A., Porcù, E., Benetton, M., Simonato, M., Simula, L., Borella, G., Polato, K., Minuzzo, S., Borile, G., et al. (2020). Thioridazine requires calcium influx to induce MLL-AF6–rearranged AML cell death. Blood Adv. *4*, 4417–4429.

Vo, T.T., Ryan, J., Carrasco, R., Neuberg, D., Rossi, D.J., Stone, R.M., Deangelo, D.J., Frattini, M.G., and Letai, A. (2012). Relative mitochondrial priming of myeloblasts and normal HSCs determines chemotherapeutic success in AML. Cell *151*, 344–355.

Waitkus, M.S., Diplas, B.H., and Yan, H. (2018). Biological role and therapeutic potential of IDH mutations in cancer. Cancer Cell *34*, 186–195.

Wunderlich, M., Mizukawa, B., Chou, F.-S.S., Sexton, C., Shrestha, M., Saunthararajah, Y., and Mulloy, J.C. (2013). AML cells are differentially sensitive to chemotherapy treatment in a human xenograft model. Blood *121*, e90–e97.

Yoshida, G.J. (2015). Metabolic reprogramming: the emerging concept and associated therapeutic strategies. J. Exp. Clin. Cancer Res. *34*, 111.

Zampini, M., Bisio, V., Leszl, A., Putti, M.C., Menna, G., Rizzari, C., Pession, A., Locatelli, F., Basso, G., Tregnago, C., et al. (2017). A three-miRNA-based expression signature at diagnosis can predict occurrence of relapse in children with t(8;21) *RUNX1 - RUNX1T1* acute myeloid leukaemia. Br. J. Haematol. 1–4.

Zhao, R., Zarabi, S., Nii, T., Halgas, O., Jitkova, Y., Ruvolo, V., Heese, L., Nishida, Y., Borthakur, G.M., Kojima, K., et al. (2019). Dual targeting of mitochondrial unfolded protein response and BCL2 in acute myeloid leukemia. Blood *134*, 2562.

Zwaan, C.M., Kolb, E.A., Reinhardt, D., Abrahamsson, J., Adachi, S., Aplenc, R., De Bont, E.S.J., De Moerloose, B., Dworzak, M., Gibson, B.E.S.S., et al. (2015). Collaborative efforts driving progress in pediatric acute myeloid leukemia. J. Clin. Oncol. *33*, 2949–2962.

STAR★METHODS

KEY RESOURCES TABLE

REAGENT or RESOURCE	SOURCE	IDENTIFIER
Antibodies		
CDK6+RUNX1 Protein Protein Interaction Ab Pair (for PLA)	Abcam	Cat# DI0411
anti-CDK6	Santa Cruz Biotecnology	Cat# scc-7961
TOMM20	Abcam	Cat# ab56783
PU1	Santa Cruz Biotecnology	Cat# sc-352
β-ACTIN	Sigma-Aldrich S.r.l.	Cat# A5316
α-TUBULIN	Sigma-Aldrich S.r.l.	Cat# T9026
GAPDH	GeneTex	Cat# GTX627408
anti-rabbit horseradish peroxidase–conjugated secondary antibody	Santa Cruz Biotecnology	Cat# sc-2357
anti-mouse horseradish peroxidase–conjugated secondary antibody	PerkinElmer	Cat# NEF822001EA
Goat anti-Mouse IgG (H+L) Cross-Adsorbed Secondary Antibody, Alexa Fluor 594	ThermoFisher Scientific	Cat# A-11032
CD34-PC7	Becton Dickinson	Cat# 348811
CD38-APC-A750	Becton Dickinson	Cat# B49200
CD33-APC	Beckman Coulter	Cat# IM2467
CD11b-PE	Beckman Coulter	Cat# IM2581U
CD15-FITC	Beckman Coulter	Cat# 332778
CD14-PC7	Beckman Coulter	Cat# A22331
CD66b-PE	Becton Dickinson	Cat# 561650
CD45-ECD	Beckman Coulter	Cat# A07784
CD16-PC5	Beckman Coulter	Cat# A07767
CD164-PerCP Cy5.5	Becton Dickinson	Cat# 561196
Lin1-FITC anti-human Lineage cocktail 1	Becton Dickinson	Cat# 340546
CD90-PC7	Becton Dickinson	Cat# 561558
CD45-RA-PE	Becton Dickinson	Cat# MHCD45RA04
CD10-PC7	Becton Dickinson	Cat# A46527
CD7-FITC	Becton Dickinson	Cat# 332773
CD135-PE	Becton Dickinson	Cat# IM2234U
CD38-eFluor450 for PrimeFlow RNA Assay	Invitrogen	Cat# 48-0389-42
CD34-APC-eFluor780 for PrimeFlow RNA Assay	Invitrogen	Cat# 47-0349-42
CDK6-AS1 RNA probe for PrimeFlow RNA Assay	Invitrogen	Cat# VA1-3024816-PF
Chemicals, peptides, and recombinant proteins		
Trizol	Invitrogen	Cat# 15596026
human GM-CSF	Milteny Biotec	Cat# 130-093-864
interleukin3 (rhIL-3)	Milteny Biotec	Cat# 130-093-909
interleukin6 (rhIL-6)	Milteny Biotec	Cat# 130-093-931
stem cell factor (rhSCF)	Milteny Biotec	Cat# 130-096-694
thrombopoietin (rhTPO)	Milteny Biotec	Cat# 130-095-747

(*Continued on next page*)

Continued

REAGENT or RESOURCE	SOURCE	IDENTIFIER
fms-like tyrosine kinase-3 ligand (rhFLT-3 ligand)	Milteny Biotec	Cat# 130-096-479
Fibronectin	Corning	Cat# 356008
methylcellulose semisolid (Methocult)	StemCell Technologies	Cat# H4230
3-[4,5-dimethylthiazol-2-yl]-2,5-diphenyltetrazolium bromide (MTT)	Sigma-Aldrich S.r.l.	Cat# M5655
Nocodazole	Sigma-Aldrich S.r.l.	Cat# M1404
RNase A	Qiagen	Cat# 1045705
ATRA (Retinoid Acid)	Sigma-Aldrich S.r.l.	Cat# R2625
Tigecycline (TIGE)	Selleckchem	Cat# S1403
Oligomycin (OLIG)	Sigma-Aldrich S.r.l.	Cat# O4876
Rotenone (ROT)	Sigma-Aldrich S.r.l.	Cat# R8875
Venetoclax (VEN) ABT-199	Sigma-Aldrich S.r.l.	Cat# ADV465750285
Enasidenib (ENA)	Selleckchem	Cat# S8205
Ivosidenib (IVO)	Selleckchem	Cat# S8206
Cytarabine (ARA-C)	Sigma-Aldrich S.r.l.	Cat# PHR1787
DAPI	Sigma-Aldrich S.r.l.	Cat# 10236276001
Hoechst33342	Invitrogen	Cat# H3570
Pyronin Y	Sigma-Aldrich S.r.l.	Cat# 83200
Latex Beads, fluorescent red	Sigma-Aldrich S.r.l.	Cat# L3030
Propidium Iodide (PI) Staining Solution	Becton Dickinson	Cat# 556463
Critical commercial assays		
SuperScript II Reverse Transcriptase	Invitrogen	Cat# 18064014
SYBR Green PCR master mix	Applied Biosystems	Cat# 4309155
Cytoplasmic & Nuclear RNA Purification Kit	Norgen biotek corp.	Cat# 21000
anti-human CD34 microbeads	Miltenyi Biotec	Cat# 130-046-702
Dual-Luciferase Reporter Assay	Promega Corporation	Cat# E1910
Duolink® In Situ Red Starter Kit Mouse/Rabbit (for PLA)	Sigma-Aldrich S.r.l.	Cat# DUO92101-1KT
CellTiter-Glo® assay	Promega Corporation	Cat# G7572
PrimeFlow RNA Assay	Invitrogen	Cat# 88-18005-204
TMRE-Mitochondrial Membrane Potential Assay Kit	Abcam	Cat# ab113852
Deposited data		
HTA expression data	Tregnago et al. (2016)	GSE75461
Microarray-based profiling of ncRNAs in normal hematopoiesis	Schwarzer et al. (2017)	GSE98633
ChIP-seq data	McKeown et al. (2017)	PRJNA381888
Experimental models: Cell lines		
SHI-1	DSMZ	Cat# ACC 645
HL-60	DSMZ	Cat# ACC 3
U-937	DSMZ	Cat# ACC 5
Experimental models: Organisms/strains		
NSG (NOD/scid IL-2Rgnull)	Charles River laboratories	005557

(*Continued on next page*)

Continued

REAGENT or RESOURCE	SOURCE	IDENTIFIER
Recombinant DNA		
Cell Line Nucleofector® Kit V	Lonza	Cat# LOVCA1003
p2CZL short hairpin RNAs (shRNAs1, 2 and 3)	Fernando et al. (2015)	provided by Dr. Rao
pGL4.28[luc2CP/minP/Hygro] luciferase vector	Promega Corporation	Cat# E8461
siRNA for *CDK6*	Invitrogen	Cat# 103566 and Cat# 118614
pHAGE-CDK6	Addgene	Cat# 116725
Software and algorithms		
R version 3.6	R Core Team	https://www.r-project.org
Prism 8	GraphPad Software	https://graphpad.com/scientific-software/prism
Fiji (ImageJ)	Open Source	https://imagej.net/software/fiji/
FlowJo v10	FlowJo LLC	https://www.flowjo.com

RESOURCE AVAILABILITY

Lead contact

Further information and requests for resources and reagents should be directed to and will be fulfilled by the lead contact, Martina Pigazzi (martina.pigazzi@unipd.it).

Materials availability

All developed expression plasmids produced in this study can be made available upon request to the lead contact.

Data and code availability

This paper analyses existing, publicly available data. These accession numbers for the datasets are listed in the key resources table. This paper does not report original code. Any additional information required to reanalyze the data reported in this paper is available from the lead contact upon request.

EXPERIMENTAL MODEL AND SUBJECT DETAILS

Patients' samples

Patients with *de novo* AML (N=132) other than acute promyelocytic leukemia, aged 0–18 years, diagnosed between 2002 and 2014 were included in this study (see Table S1A). These children were treated according to the same protocol, namely the AIEOP AML 2002/01. FAB morphological classification, immunophenotypic analysis and molecular characterization were centrally reviewed. Bone marrow (BM) samples were processed for RNA isolation and PCR analysis. PCR for recurrent rearrangements, such as those involving *CBF*, *MLL*, *FLT3*, and other rare mutations, were performed (Masetti et al., 2013; Pigazzi et al., 2011, 2012). In accordance with the Declaration of Helsinki, informed consent to provide samples for biological studies was obtained from patient's parents or legal guardians.

Cell lines

SHI-1 leukemia cell line was bought at DSMZ-Collection of Microorganisms and Cell Cultures, Germany and cultured in DMEM 10% FBS (Invitrogen, Carlsbad, CA) for around 20-30 passages (maximum) from thawing. Analogously HL-60 and U-937 were cultured in RPMI 10% FBS (Invitrogen, Carlsbad, CA). Mycoplasma absence was tested using a commercial kit (Minerva Biolabs, Berlin, DE).

Primary cell cultures

Human CB was collected after obtaining a written informed consent for research use from the delivering women. Mononuclear cells were isolated from CB samples by density gradient centrifugation at 400 g for 20 min, using Ficoll solutions. In order to isolate CD34+ and CD34− cells, samples were incubated with anti-human CD34 microbeads. Primary healthy CD34+ cells were cultured in RPMI1640 10% FBS supplemented with recombinant human (rh) cytokines: interleukin6 (rhIL-6; 20 ng/mL), stem cell factor (rhSCF;

100 ng/mL), thrombopoietin (rhTPO; 20 ng/mL) and fms-like tyrosine kinase-3 ligand (rhFLT-3 ligand; 100 ng/mL).

Primary AML cells were cultured in RPMI1640 10% FBS with the addition of recombinant human (rh) cytokines: interleukin3 (rhIL-3; 20 ng/mL), rhIL-6; 20 ng/mL, rhSCF; 50 ng/mL, rhTPO; 50 ng/mL and rhFLT-3 ligand (50 ng/mL) (Tregnago et al., 2020). All cell cultures were maintained at 37°C, 5% CO_2.

Animal models

Procedures involving animals and their care were in accordance with institutional guidelines that comply with national and international laws and policies (EEC Council Directive 86/609, OJ L 358, 12 December 1987) and with "ARRIVE" guidelines (Animals in Research Reporting In Vivo Experiments). Ministry authorization approved: 622/17-PR, 512/19-PR. NSG mice (of 4-8 weeks old, randomized for sex, 20-25 g/mouse, maximum 5 animals/cage) were injected intravenously (tail vein) with $1x10^6$ human CD45 (hCD45) cells derived from PDX-P3 (biobank).

METHOD DETAILS

Quantitative real-time PCR

Total RNA was isolated using Trizol. One microgram RNA was reverse-transcribed into cDNA using SuperScript II. Expression of mRNA were measured by Real Time PCR (RQ-PCR) on an ABI 7900HD platform (Applied Biosystems, Foster City, CA) using the SYBR Green PCR master mix and normalized on *GUSB* using the 2^-ΔΔCt method. Cytoplasmic & Nuclear RNA Purification Kit was used for cytoplasmic or nuclear RNA fractionation. Ratio were calculated as $2^{-(Ct\ cytoplasmic-\ Ct\ nuclear)}$ (Schwarzer et al., 2017).

GEP and correlation analyses

RNA from bone marrow (BM) cells collected at diagnosis from 58 patients was hybridized on the GeneChip® Human Transcriptome Array 2.0 (HTA, Affymetrix, Santa Clara, CA, USA). Microarray expression data are deposited in GEO database under accession number GSE75461(Tregnago et al., 2016).

Briefly, 100 ng of total RNA were labeled and hybridized to Affymetrix GeneChip for 16 h at 45°C using a rotational oven and washed according to Affymetrix standard protocols using a GC450 Fluidics Station. RNA quality was assessed on an Agilent2100 Bioanalyzer (Agilent Technologies).

The GeneChips were scanned with an Affymetrix 7G scanner and the CEL files generated were analyzed through Affymetrix Expression Console Software (version 1.3) which normalizes array signals using a robust multiarray averaging (RMA) algorithm. Probes were re-annotated using GENECODE v.19 gene annotation database (www.genecodegenes.org) in order to identify both coding and non-coding RNAs covered by probes. Transcripts were included if at least the 95% of nucleotides overlapped with probes. In miRNAs analysis, for every probe which recognizes pre-miRNA, we used both associated mature miRNA, where available. Normalized data were analyzed using GENE-E analysis platform (Broad Institute of Harvard and MIT, Boston, MA). Arraystar Human LncRNA microarray V2.0 probes (GPL23434 platform) were mapped to RefSeq genes. Microarray expression data are deposited in GEO database under accession number GSE75461 (Tregnago et al., 2016).

Coding and noncoding gene expression data of human blood cells from healthy donors were downloaded as Series Matrix File of the GSE98633 dataset (Schwarzer et al., 2017) from the GEO database. Thirty-three samples from the dataset were selected and distinguished into "mature Granulocytes purified from peripheral blood", "CD14+ Monocytes purified from peripheral blood", "purified erythroblasts *in vitro* derived", "purified megakaryocytic progenitors *in vitro* derived", "CMP purified from cord blood", "GMP purified from cord blood", "CD34+ CD38- HSPC purified from cord blood", "CD14+ CD38- HSCP purified from fetal liver" and "G-CSF-mobilized CD34+ CD38-HSCP purified from peripheral blood".

For *CDK6-AS1* interaction network from gene expression data, we ranked the genes according to their absolute Spearman's rank correlation coefficient across all the selected samples with the expression profile of the probe detecting the first exon of both *CDK6* and *CDK6-AS1* genes, using the 'cor' function within the 'stats' package of the R software. The top 1% correlated values associated to 251 probes, and mapping to

337 RefSeq transcripts, were then used to perform an unsupervised clustering by using GSE98633 dataset (Schwarzer et al., 2017).

Unsupervised clusterings were created using the 'heatmap.plus' function from the heatmap.plus' R package with the 'canberra' as distance method and 'ward.D2' as the clustering algorithm and visualized using the 'heatmap3' function from the 'hetamap3' package.

Boxplots were produced using the 'boxplot' function of the 'graphics' R package with the Wilcoxon test p-values calculated by means of the 'wilcox.test' function of the 'stats' package.

For each sample from PRJNA381888 (McKeown et al., 2017) and GSE75461 (Tregnago et al., 2016) datasets, expression and ChIPseq signals within 5 Mb from the *CDK6/CDK6-AS1* genes were firstly mapped within overlapping 100 kb intervals and the resulting binned values were subsequently correlated to the value of the bin harboring the *CDK6/CDK6-AS1* shared exon1. Smoothed averages were calculated using the 'smooth.spline' function form the 'stats' R package.

t-SNE

Dimensionality reduction clustering by means of t-distributed stochastic neighbor embedding (t-SNE) was performed using the 'Rtsne' function of the 'Rtsne' R package after calculating inter-samples distances with the 'dist' function of the 'stats' R package by means of the 'maximum' distance method and plotted using the 'plot' function of the 'graphics' R package.

Gene Set Enrichment Analysis (GSEA)

GSEA was performed using the 'Signal2Noise' metric for ranking genes and tested against the c5.all.v6.2.symbols.gmt Gene Ontology sets database with 5000 permutations and a 'weighted_p2' enrichment statistic. A leading edge analysis was then performed on the resulting gene sets hits showing both nominal p-values lower than 0.05.

Cell treatments

Cells were treated with Tigecycline (TIGE), Oligomycin (OLIG) Rotenone (ROT), Venetoclax (VEN), Enasidenib (ENA), Ivosidenib (IVO), Cytarabine (ARA-C) for dose-response evaluation. After GI_{50} calculation, cells were treated with 0.6 μM of ARA-C, 60 μM of TIGE or COMBO (ARA-C+TIGE).

Cell transfection and lentiviral transduction

Three specific p2CZL short hairpin RNAs (shRNAs1, 2 and 3) were kindly provided by Dr. Rao (Fernando et al., 2015) and used to silence *CDK6-AS1* both transiently (pool of three) and stably.

Transient cell transfection was performed using the Cell Line Nucleofector® Kit V.

Two specific siRNAs, one mapping at 3'UTR and one in the coding region, were adopted to silence *CDK6*. We used the combination of the two oligos for a better silencing effect. Transfected cells were screened by RQ-PCR for *CDK6* and *CDK6-AS1* expression, CDK6 protein level was checked by western blot, and cells were used for *in vitro* experiments.

Third-generation lentiviral vectors were produced to generate *CDK6-AS1* stable knockdown constructs (Fernando et al., 2015). A total of $14x10^6$ SHI-1 and $1x10^6$ CD34+ cells were spin-infected at 37°C overnight in the presence of polybrene 8 μg/ml (Manara et al., 2014). Transduced cells were single-cell sorted for GFP expression (MoFlow XDP FACS (Beckman Coulter, Brea, CA). Cells were screened by RQ-PCR for *CDK6-AS1* expression and best clones were selected for expansion and *in vitro* experiments: we referred to shRNA 1 colony 2 (namely "shCDK6-AS1") for the best downregulation of both *CDK6-AS1* and *CDK6*, but other independent clones were used and presented in Supplemental Figures.

Plasmids construction

For CDK6 overexpression, we generated a new construct starting from pHAGE-CDK6 plasmid (gift from Gordon Mills & Kenneth Scott (Ng et al., 2018)) and pEGFP-N1 (Pigazzi et al., 2008). In detail, we cut pHAGE-CDK6 with NcoI and pEGFP-N1 with EcoRI, used DNA Polymerase I Large (Klenow) Fragment

(Promega) to generate blunt ends, then cut both plasmids using NotI. After this second digestion, we subcloned the *CDK6* fragment into pEGFP-N1 backbone, obtaining pCDK6 plasmid. Both pCDK6 and pEGFP-N1, used as control vector and indicated as pØ, were transiently transfected in SHI-1 cell line for *in vitro* validations.

Plasmids construction and promoter activity assay

We generated reporter vectors to verify CDK6/*CDK6-AS1* bidirectional promoter activity. By *in silico* prediction, we selected a 1.17 kb genomic fragment of chromosome 7 (hg19: 5'-92464746-92465919-3'), amplified it using a pair of primers including the restriction sites for XhoI and HindIII (Forward primer-XhoI CTCGAGAGAGAAACGGGAGCAGCAATG, Reverse primer-HindIII AAGCTTCCGGAGAGAGTGCTGG TAAC), and cloned it into the pGL4.28[*luc2CP*/minP/Hygro] luciferase vector, obtaining pGL4-CDK6-AS1/CDK6-LUC plasmid. We subsequently constructed the double luciferase vector, by amplifying the *luc2CP* gene of the pGL4.28 (Forward primer-KpnI GGTACCCCCGACTCTAGACTGCAGTT, Reverse primer-NheI GCTAGCGGCAATCCGGTACTGTTGGT) and cloning it in 3'-5' direction upstream the promoter region, obtaining pGL4-LUC-CDK6-AS1/CDK6-LUC plasmid. Then, we knocked-out *luc2CP* gene from the pGL4-CDK6-AS1/CDK6-LUC plasmid, by mutagenesis of the ATG start codon (Q5® site-directed mutagenesis Kit, New England BioLabs, Ipswich, MA - Forward primer AAGATGCCAAAAACATTAA GAAG, Reverse primer ATGGTGGCTTTACCAACAG), producing the pGL4-CDK6-AS1/CDK6-ΔLUC plasmid. To test luciferase activity, we transfected SHI-1 shNEG and shCDK6-AS1 stable cell lines with 0,6 μg of each of these vectors, together with 0.06 μg of Renilla, using the Nucleofector system, and measured luciferase activity 6 hours after transfection (Dual-Luciferase Reporter Assay).

RNA detection by flow cytometry

To investigate the expression of *CDK6-AS1* in primary AML samples by flow cytometry, we took advantage of the PrimeFlow RNA Assay, an innovative technique consisting of an *in situ* hybridization to detect RNA transcripts together with cell surface markers by flow cytometry. Following manufacturer's instructions, cells were stained for the surface markers using anti-CD34 and CD38 antibodies. Next, cells were fixed and permeabilized to allow the binding of the target RNA probe for *CDK6-AS1* to its specific transcript inside the cell. Cells were analyzed by flow cytometry by gating on CD34+/CD38- cells to evaluate the median fluorescence intensity for *CDK6-AS1*.

Cell viability and cell cycle

Cell viability assays were performed using CellTiter-Glo® assay. Briefly, 5×10^4 cells were cultured in sterile 96-well plates and incubated for 24 to 48 hours; then, 90 μl of CellTiter-Glo® reagent was added and after 15-minute incubation at room temperature, luminescence was recorded (VICTOR, Perkin Elmer, Milan, IT) with an integration time of 1s per well. The combination index (CI = (Drug1 effect + drug2 effect) / combo effect (Foucquier and Guedj, 2015)) was calculated to evaluate the synergistic effect (CI<1). For cell-cycle analyses, 16-hour incubation with 300 nM nocodazole was used to synchronize in G2/M phase. The synchronized cells were washed with PBS and released from the mitotic block by the addition of normal serum-containing media and fixed in 70% cold-ethanol for at least 1 hour at −20°C. Fixed cells were incubated in propidium iodide (PI) staining buffer (PBS containing RNase A (50 μg/ml), 0.1% sodium citrate, and PI (50 μg/ml) for 30 minutes at room temperature (RT). Cells were analyzed by flow cytometry and the cell distribution was determined using the FlowJo software.

Cell differentiation

Differentiation markers were detected by flow cytometry. Phagocytosis capability was assessed adding Latex Beads at a ratio of 1:500 with or without the addiction of 30 ng/ml GM-CSF. Cells were analyzed by flow cytometry and representative images were captured after centrifugation by cytospin or seeding cells on fibronectin (40 μg/ml)-coated chamber slides and stained by May–Grünwald Giemsa method.

At the indicated times, cells were measured by flow cytometry for the expression of CD11b and CD16 after 24-48 hours of *CDK6-AS1* or *CDK6* knockdown (Tregnago et al., 2016). Normal CD34+ cells were analyzed for surface markers expression by staining with CD34, CD38, CD164, Lin1 (anti-human Lineage cocktail 1, including CD3, CD14, CD16, CD19, CD20, CD56), CD90, CD45RA, CD33, CD66b, CD10, CD7, CD15, CD135.

Colony forming assay

After *CDK6-AS1* silencing, a total of 2×10^3 SHI-1 cells were seeded onto a minimum methylcellulose semi-solid dish (Methocult) and incubated at 37°C. Fourteen days later, colonies were counted by light microscopy after incorporation of 3-[4,5-dimethylthiazol-2-yl]-2,5-diphenyltetrazolium bromide (MTT).

Cell quiescence

Hoechst33342 and Pyronin Y staining was used to discriminate quiescent cells, in G0 phase (Hoechst-/Pyronin Y-), with respect to G1 and S-G2/M phases, in TMRE-sorted normal CD34+ cells. After cell sorting, cells were incubated with Hoechst33342 10 μg/ml and Pyronin Y 3 μg/ml, for 45 and 15 minutes respectively.

Mitochondrial mass quantification

Immunofluorescence was performed either in cytospins of transient or stable *CDK6-AS1* knockdown cells cultured in suspension or in chamber slides after 30 minutes of fibronectin (40 μg/ml) coating at 37°C. Cells were incubated overnight at 4°C with primary antibody anti-TOMM20 to visualize mitochondria and then with goat anti-mouse IgG (H+L) secondary Antibody, Alexa Fluor 594 for 1h. DAPI/Hoechst 33342 were used to label nuclei. Images were acquired using confocal microscope ZEISS LSM800. The mitochondrial area was quantified using Fiji-ImageJ.

Mitochondrial membrane potential

TMRE-Mitochondrial Membrane Potential Assay Kit was used for measuring the mitochondrial membrane potential. Briefly, TMRE 200 nM diluted in BSA 0.2%-PBS 1x was added at 37°C. After 20' incubation, cells were analyzed by flow cytometry using Cytomic FC500 or CytoFLEX. Normal CD34+ cells were sorted for TMRE MFI levels (MoFlow XDP FACS, Beckman Coulter, Brea, CA).

PLA analysis

In situ proximity ligation assay (PLA) experiments were performed by using DuoLink II. Cells were incubated overnight at 4°C with anti-RUNX1 and anti-CDK6 antibody in diluent buffer. Samples were then washed with PLA washing buffer and incubated with PLA probes anti-rabbit-PLUS and anti-mouse-MINUS. The subsequent washing steps, ligation, rolling-circle amplification and fluorescent labeling with DuoLink II Detection Reagent Red were performed according to the manufacturer's instructions. Slides were mounted in vector shield Mounting Media with DAPI; Zeiss LSM 510 microscope equipped with a Zeiss image processing system was used for confocal imaging analysis processed with identical settings for all conditions.

Immunoblotting

Equal amounts of proteins (10 μg) were resolved by SDS PAGE gels and transferred to polyvinylidene difluoride (PVDF) membrane. After blocking for at least 1 h at room temperature, membranes were incubated overnight at 4 °C with primary antibodies anti-β-ACTIN, anti-GAPDH, anti-α-TUBULIN, anti-CDK6, TOMM20 and then incubated with horseradish peroxidase-labeled secondary antibodies, either anti-rabbit or mouse, for 60 min. All membranes were visualized using ECL Select and exposed to iBright FL1500 (ThermoFisher) (Bisio et al., 2017). Signal was quantified by Fiji-ImageJ software.

In vivo experiments

NSG mice (of 4-8 weeks old, randomized for sex) were injected intravenously (tail vein) with $1x10^6$ human CD45 (hCD45) cells derived from PDX-P3 (biobank). After 1 month from leukemic cell injection, tumor burden was assessed weekly by flow cytometric measurement of hCD45 positive cells in peripheral blood (PB). Treatment was delayed until leukemia burden was around 5% in PB. For the *in vivo* experiment performed using shNEG and *CDK6-AS1* KD cell line, NSG mice were injected intravenously with $1.5x10^6$ cells and treatments started after 5 days from cells inoculation. Mice were randomized into 4 groups (n=3/5) and treated with TIGE 75 mg/kg, ARA-C 25 mg/kg (low dose), combination of TIGE 75 mg/kg +ARA-C 25 mg/kg (COMBO), and control group (DMSO). Drugs were given daily with weekend wash out (for three weeks in PDXs, whereas mice injected with SHI-1 were treated for two weeks), by intraperitoneal (i.p.) injection. Treatment efficacy was assessed by flow cytometric measurement of hCD45 positive cells; in particular for PDXs we evaluated peripheral blood (PB), whereas SHI-1-injected mice were evaluated at sacrifice for BM invasion and spleen dimension. TIGE and ARA-C powder were dissolved in DMSO to prepare stock solutions that were freshly diluted in saline solution for i.p. injection. Appropriate vehicle was used for

control group. Mice weight was monitored twice a week in order to adjust the correct dose of drugs during treatment.

QUANTIFICATION AND STATISTICAL ANALYSIS

Statistical analyses

The t-test was adopted for detecting significance between differences in means; the Wilcoxon test was used as a non-parametric alternative to the Student's t-test. Overall survival was estimated using the Kaplan–Meier method and differences between groups were compared through the log-rank Mantel-Cox test. Graphs and associated statistical analyses were generated using GraphPad Prism 8. All data are presented as mean±standard error of the mean (SEM). *p-value<0.05, **p-value<0.01, ***p-value<0.001, ****p-value<0.0001 were considered to be statistically significant.